Deep-Sea Research II 116 (2015) 208–225

Contents lists available at ScienceDirect

Deep-Sea Research II

journal homepage: www.elsevier.com/locate/dsr2

Dynamic variability of dissolved Pb and Pb isotope composition from the U.S. North Atlantic GEOTRACES transect

Abigail E. Noble [a,1], Yolanda Echegoyen-Sanz [b], Edward A. Boyle [a,*], Daniel C. Ohnemus [c], Phoebe J. Lam [c], Rick Kayser [a], Matt Reuer [a], Jingfeng Wu [d], William Smethie [e]

[a] Massachusetts Institute of Technology, Cambridge, MA, USA
[b] Universidad de Zaragoza, Zaragoza, Spain
[c] Woods Hole Oceanographic Institution, Woods Hole, MA, USA
[d] Rosentiel School of Marine and Atmospheric Science, University of Miami Miami, Coral Gables, FL, USA
[e] Lamont-Doherty Earth Observatory, Columbia University, Palisades, NY, USA

ARTICLE INFO

Available online 2 December 2014

Keywords:
GEOTRACES
Lead
Pb
Lead isotopes
North Atlantic Ocean
Trace elements
Anthropogenic

ABSTRACT

This study presents dissolved Pb concentration and isotopic composition distributions from GEOTRACES GA03, the U.S. North Atlantic Transect. Pb in the ocean is primarily derived from anthropogenic sources and Pb fluxes into the North Atlantic Ocean have been steadily decreasing following the phase-out of alkyl leaded gasoline usage in North America and Europe between 1975 and 1995. A compilation of dissolved Pb profiles from three stations occupied repeatedly during the last three decades reveals a dramatic decrease in concentrations within the surface layers and the thermocline maxima, although elevated concentrations greater than 60 pmol/kg are still observed in the center of the North Atlantic gyre where ventilation timescales are longer than at the western boundary. The evolution of stable Pb isotopes at these stations shows a shift from dominantly North American-like composition in surface waters in the early 1980s towards a more European-like composition in later years. The most recent shallow signatures at the Bermuda Atlantic Time Series station (BATS) show an even more recent trend returning to higher $^{206}Pb/^{207}Pb$ ratios after the completed phase-out of leaded gasoline in Europe, presumably because recently deposited Pb is more strongly influenced by industrial and incineration Pb than by residual alkyl leaded gasoline utilization. In surface waters, trends toward a more prominent European influence are also found in the middle of the basin and toward the European coast, coincident with higher concentrations of surface dissolved Pb. Scavenging of anthropogenic Pb is observed within the TAG hydrothermal plume, and it is unclear if there is any significant contribution to deep water by basaltic Pb leached by hydrothermal fluids. In the upper water column, many stations along the transect show Pb concentration maxima at ~100 m depth, coincident with a low $^{206}Pb/^{207}Pb$ isotopic signature that is typical of European emission sources. Although Pb ores from the United States historically tend to carry $^{206}Pb/^{207}Pb$ signatures >1.17 (Hurst, 2002), subsurface signatures as low as 1.1563 in $^{206}Pb/^{207}Pb$ were observed in this feature. This signature appears to be carried westward within saline Subtropical Underwater (STUW), that ventilates from the Central Eastern part of the North Atlantic Subtropical Gyre where the lowest surface isotope $^{206}Pb/^{207}Pb$ ratios are observed. Along the western boundary, deep water masses of different ages carry distinct isotope ratios corresponding to their respective times of ventilation. Finally, a low $^{206}Pb/^{207}Pb$ signature in bottom water along the Eastern margin suggests that there may be some mobilization of European-derived anthropogenic Pb from recent surface deposits on the ocean floor.

1. Introduction

The evolving distribution of Pb within the ocean provides a case study of the far-reaching footprint of humans on the environment. In the recent past, the North Atlantic Ocean was historically the most strongly affected basin, receiving a large atmospheric flux of Pb during the last several decades from industrial activities and especially from leaded gasoline utilization in the US and Europe.

* Corresponding author.
E-mail address: eaboyle@mit.edu (E.A. Boyle).
[1] Present address: Environmental Chemistry Group, Gradient, 20 University Road, Cambridge, MA 02138, United States.

http://dx.doi.org/10.1016/j.dsr2.2014.11.011
0967-0645/

Most of the Pb in the oceans is derived from anthropogenic sources with leaded gasoline being the largest source during its peak utilization, and high temperature industrial processes such as coal burning, smelting, and incineration also contributing to this flux (Nriagu, 1979). Pb reaches the ocean through the advection and deposition of fine atmospheric aerosols, and many studies have focused on characterizing the Pb isotopic signature of aerosols and rain from different source regions that affect the North Atlantic Basin (Hamelin et al., 1997; Véron et al., 1998, 1992; Véron and Church, 1997; Kumar et al., 2014; Erel et al., 2007; Church et al., 1990). Changes in the flux of Pb to the ocean over time have been recorded by incorporation into sediments, corals, and snow (Schaule and Patterson, 1983; Trefry et al., 1985; Shen and Boyle, 1988; Véron et al., 1987; Hamelin et al., 1990; Boyle et al., 1994; Callender and Van Metre, 1997; Reuer et al., 2003; Kelly et al., 2009). The consequences of these fluxes on the Atlantic Ocean Pb distribution have been documented in several publications (Boyle et al., 1986; Shen and Boyle, 1988; Helmers et al., 1990, 1991; Helmers and van. der. Loeff, 1993; Véron et al., 1993, 1994, 1999; Hamelin et al., 1997; Wu and Boyle, 1997; Alleman et al., 1999; Weiss et al., 2003). During the past 200 years, the evolution of Pb in surface waters of the Western North Atlantic has shown a steady increase in concentration during the industrial revolution and a rapid rise after the introduction of alkyl leaded gasoline in the 1920s followed by a dramatic decrease after the phaseout of Pb gasoline usage in the 1970s and 1980s (Shen and Boyle, 1988; Desenfant et al., 2006; Kelly et al., 2009). The changing surface concentrations are injected into the ocean interior by thermocline ventilation and deepwater formation, and elevated concentrations are still found in intermediate level waters that were injected during previous decades when North Atlantic surface Pb concentrations were an order of magnitude higher than today (Boyle et al., 1986; Alleman et al., 1999; Véron et al., 1999). Early work has shown that the majority of Pb delivered to the Atlantic Ocean interior occurs through lateral ventilation of thermocline waters rather than through vertical processes (Boyle et al., 1986; Shen and Boyle, 1988). During the past four decades, as both the US and Europe have phased out the usage of alkyl leaded gasoline, Pb concentrations in the ocean surface and interior have decreased dramatically. This decrease is driven both by the decreased flux of Pb into the oceans and by scavenging onto sinking particles within the water column. The Pb residence time is ~2 years in oligotrophic surface waters and decades to a century in deeper waters (Bacon et al., 1976; Nozaki et al., 1976). In surface waters, steady-state balance is achieved between input and particle uptake, therefore surface water Pb tracks inputs. It is not known whether shallow Pb removal occurs by active biological uptake or passive scavenging onto particle surfaces, but in deeper waters, it is attributed to passive scavenging.

In tandem with Pb concentration distribution, the stable Pb isotopic composition can be used to delimit time and space dependent inputs to the ocean, constraining different sources and different periods of Pb deposition. This is possible because there will be no significant interference from stable isotopic fractionation during industrial processing or in the environment in comparison to very large differences resulting from distinctive radiogenic signatures of Pb ores. Although stable isotope fractionations have been reported for some heavy stable isotopes (e.g. Tl, Rehkamper et al., 2002; Hg, Bergquist and Blum, 2007), these fractionations are at most only a few parts per thousand, whereas naturally-occurring radiogenic $^{206}Pb/^{207}Pb$ isotope signatures can vary by more than 300 parts per thousand. Lead ores contain distinctive isotopic ratios because of the temporal evolution of their parent rock U and Th reservoirs (Doe, 1970), and atmospheric and oceanic Pb inputs have changed both temporally and spatially (Schaule and Patterson, 1981, 1983). Hence, temporal and spatial source aspects of Pb transport through the ocean can be traced. The temporal evolution of Pb isotope ratios of sources can allow for determination of Pb transit times from the surface to the deep ocean (Alleman et al., 1999; Véron et al., 1999), and the naturally-occurring radioisotope ^{210}Pb enhances our ability to constrain Pb behavior on a decadal scale (Bacon et al., 1976; Turekian, 1977; Boyle et al., 1986; Shen and Boyle, 1988). Because Pb is affected by many processes that influence other trace metals (atmospheric deposition, biological uptake, and abiotic scavenging), the study of Pb not only elucidates anthropogenic contamination but also helps constrain processes that move other metals through the ocean.

This manuscript presents results from the US North Atlantic GEOTRACES Transect GA03 and examines how the distributions of Pb have changed with time by comparing these results to previous occupations of three stations. This expedition was a part of the International GEOTRACES Program, whose goal is to map the world oceans for trace elements and isotopes in order to improve our understanding of biogeochemical cycling and circulation in the ocean (www.geotraces.org).

2. Methods

Samples were collected from GEOTRACES track GA03, referred to as the U.S. GEOTRACES North Atlantic Transect (USGT-NAT), that took place in two legs, aboard the R/V *Knorr* (USGT10, Oct. 14, 2010-Nov. 3, 2010; USGT11, Nov. 4, 2011-Dec. 14, 2011; Chief Scientists: William Jenkins, Ed Boyle, and Greg Cutter). The first leg (USGT10) departed from Lisbon, Portugal and sampled Mediterranean Outflow Water (MOW) at Station USGT10-01, followed by an approximately meridional transect southwards to 21°N (Station GT10-08, Fig. 1). Because of ship malfunction, the cruise was terminated after a short zonal transect was completed across the Mauritanian Upwelling along 17.4°N (Stations USGT10-09 to USGT10-12), sampling the northern edge of the low oxygen waters there and concluding at 24.5°W, Station TENATSO (USGT10-12). The second leg (USGT11) departed from Woods Hole, MA and sampled 7 stations along Line W to the Bermuda Atlantic Time Series station (BATS, Station USGT11-10, Fig. 1). Stations were then occupied at approximately 3° spacing across the basin alternating between full depth sampling of the water column (even numbered stations) and intermediate sampling to 1000 m (odd numbered stations). Full depth stations during the two legs consisted of either 24 ("full" stations) or 36 ("super" stations) depths, and shallow stations consisted of 12 depths. A surface towed fish was also deployed and an additional surface sample was taken for each station. The second leg concluded with a re-occupation of Station TENATSO (USGT11-24).

2.1. Trace metal sampling techniques

Samples were collected using the ODU GEOTRACES Carousel (Cutter and Bruland, 2012), and were filtered through 0.2 μm Acropak capsule filters in the GEOTRACES clean van. The carousel was used to collect samples from surface to near bottom waters, and an additional sample was collected from a surface towed "fish" at each station. Pre-conditioned, teflon-coated Go-Flo sampling bottles (General Oceanics, Miami, FL) of 12 L capacity were deployed on a polyurethane powder-coated aluminum rosette with titanium pylons and pressure housings (Sea-Bird Electronics, Inc., Bellevue, WA) attached to a Kevlar, non-metallic conducting cable. For more information regarding carousel deployment, please refer to the GEOTRACES Cookbook, located on the GEOTRACES Program website (www.GEOTRACES.org). After retrieval of the carousel, Go-Flo bottles were moved to the U.S. GEOTRACES Program class-100 trace metal clean van, and pressurized with HEPA filtered air for sampling in

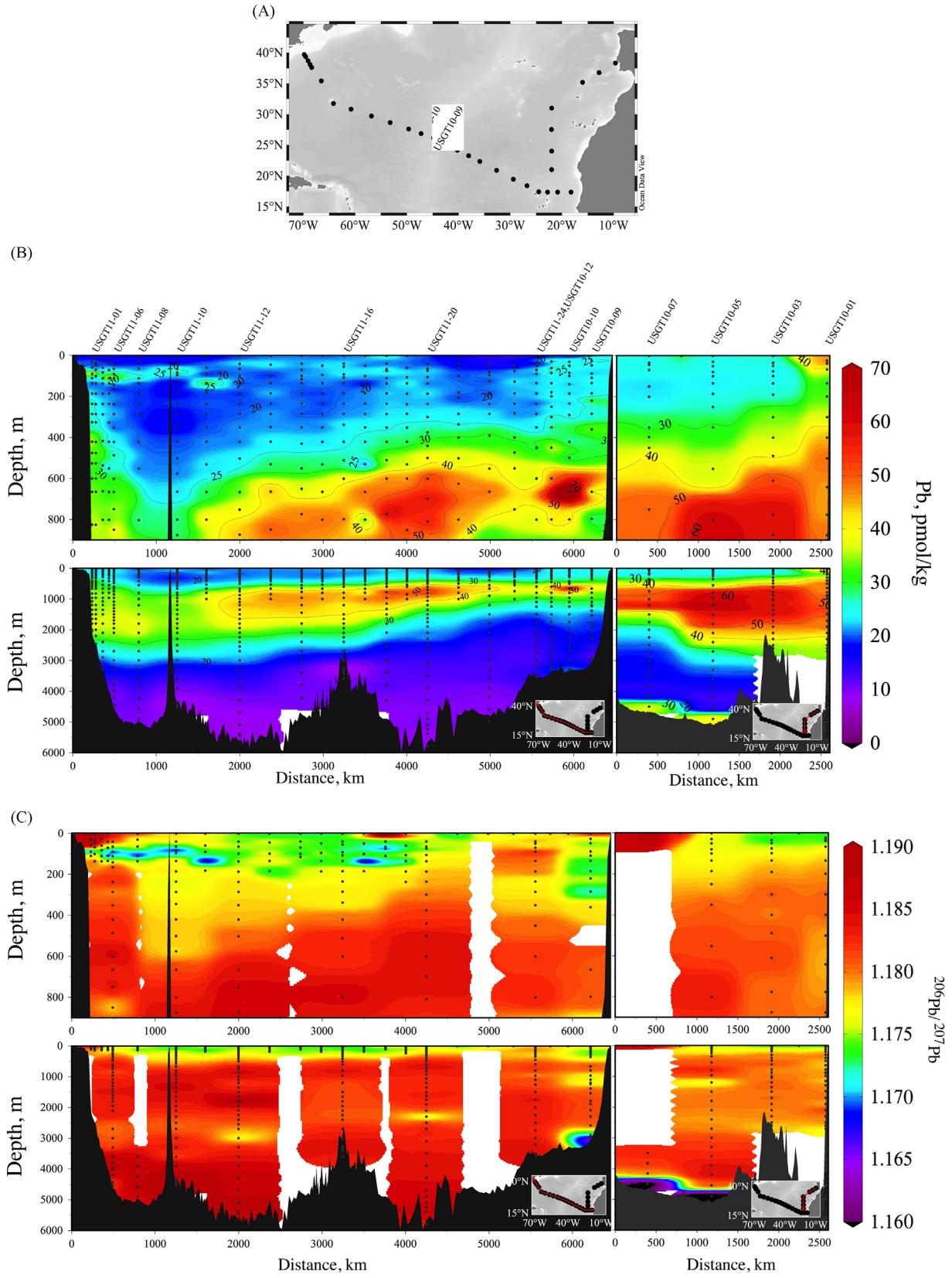

Fig. 1. (A) Map of the two US GEOTRACES North Atlantic Zonal Transect Stations, USGT10 and USGT11. Stations occupied during the 2010 effort were along the western margin of Europe and Africa, and within the Mauritanian Upwelling. Stations occupied during the 2011 effort followed a transect from Woods Hole, MA, USA across the North Atlantic, and concluding at timeseries station TENATSO. (B) Sections of dissolved Pb. The upper panels highlight more fine features observed in the upper 800 m of the water column while the lower panels show the full depth section. The left panels show the zonal transatlantic section, while the right panels show the meridional eastern basin stations. (C) Sections of stable Pb isotope ratios $^{206}Pb/^{207}Pb$. The panels follow the same scheme as the dissolved section, highlighting the upper water column features, particularly that of STUW.

accordance with published methods (Cutter and Bruland, 2012). Samples were collected into acid-washed 2 L HDPE bottles (Nalgene) and acidified onboard by the addition of 4 mL of 6 M high purity hydrochloric acid. Samples were kept at room temperature and the bottles were labeled with a sticker taken from the sampling GOFlo (allocated GEOTRACES number). Surface towed fish samples were collected by suspending the towed fish off starboard with a boom, and sampled water at approximately 2 m depth using a Teflon diaphragm pump following the GEOTRACES Program Cookbook sampling recommendations.

Before the cruise, sample storage bottle lids and threads and exterior were soaked overnight in 2 M reagent grade HCl, then filled with 1 M reagent grade HCl, heated in an oven at 60 °C overnight, rotated top to bottom, heated for a second day, and rinsed 5 times with pure distilled water. The bottles were then filled with trace metal clean dilute HCl (~0.01 M HCl) and again heated for two days in the oven, rotating top to bottom after the first day. These clean sample bottles were emptied, and double-bagged prior to rinsing and filling with filtered seawater.

2.2. Pb concentration analyses

Samples were analyzed using a 400 μL/min nebulizer with a quadrupole ICPMS (VG PlasmaQuad 2+). Concentration analyses were assessed using isotope dilution, following a previously published method (Lee et al., 2011). Briefly, samples were poured into 1.5 mL polyethylene vials (Eppendorf™ AG) in triplicate. Each sample was quantitatively pipetted to 1.3 mL with the remaining solution removed from the vial. Pipettes were calibrated daily. 25 μL of a ^{204}Pb spike was added to each sample, and the pH was raised to 5.3 using a trace metal clean ammonium acetate buffer, prepared from redistilled acetic acid and vapor-purified NH_3 solution to a pH of between 7.9 and 7.98. ~2400 beads of NTA Superflow™ resin (Qiagen Inc., Valencia, CA) were added to the mixture, and the vials were set to shake on a shaker table for 4 days to allow the sample to equilibrate with the resin. After 4 days, the beads were centrifuged and washed 3 times with pure distilled water, using a trace metal clean syphon tip to remove the supernatant water wash from the sample vial after centrifugation. After the last wash, 250 μL of a 0.1 M trace metal clean HNO_3 was added to the resin to elute the metals, and samples were allowed to sit for 2 days prior to analysis by ICP–MS. Qiagen NTA Superflow® resin was cleaned by batch rinsing with 0.1 M trace metal clean HCl for a few hours, followed by multiple washes until the pH of the solution was above 4. Resin was stored at 4 °C in the dark until use, though it was allowed to come to room temperature prior to addition to the sample. Eppendorf™ polyethylene vials were cleaned by heated submersion for 2 days at 60 °C in 1 M reagent grade HCl, followed by a bulk rinse and 4× individual rinse of each vial with pure distilled water. Each vial was then filled with trace metal clean dilute HCl (~0.01 M HCl) and heated in the oven at 60 °C for one day on either end. Vials were kept filled with this weak pure acid until just before use. 12 blanks were run for each analysis day. Averaged blanks for a given day of analyses were 4.3 ± 1.7 pmol/kg (n=8 analysis days) for the 2010 effort and 2.2 ± 0.8 pmol/kg (n=22 analysis days) for the 2011 effort. The difference between the two averages may be attributable to a transition from the use of a 0.5 N HNO_3 resin leach (2010 leg analyses), to a 0.1 N HNO_3 resin leach (2011 leg analyses). During a single batch's ICPMS run, the reproducibility of the blank is about 0.5 pmol/kg. Each sample was analyzed in triplicate. In some cases, one of the triplicate analyses was discarded if two of the three values were more similar, but the third significantly increased the RSD%. In some cases, analyses were repeated if a value appeared to be anomalously higher or lower than adjacent samples in the water column. At least one and sometimes three internal lab seawater standards were run every day on the instrument to ensure consistency between analysis days and to assay for potential contamination. On a few days, these analyses and replicates from different days indicated offsets of up to 6% from the long-term average, and the Pb concentration data for those days were adjusted accordingly. SAFe standards and GEOTRACES standards were also run and the values for D1 (22.7 ± 1.2 pmol/kg, n=3), S1 (45.9 ± 2.2 pmol/kg, n=2), GD (26.7 ± 2.2 pmol/kg, n=3), and GS (41.7 ± 1.7 pmol/kg, n=3) were consistent with the consensus values published on the GEOTRACES website (D1—27.7 ± 2.6 pmol/kg, S1—48.0 ± 2.2 pmol/kg, GD—28.6 ± 1.0 pmol/kg, GS—42.7 ± 1.5 pmol/kg, http://www.geotraces.org/science/intercalibration/322-standards-and-reference-materials).

2.3. Pb isotope analyses

Samples were analyzed on a Micromass IsoProbe ICP–MS with the use of an APEX desolvator and a 40 μL/min Micromist glass nebulizer. The overall procedure is slightly modified from a previously published protocol (Reuer et al., 2003 using column chemistry based on Krogh, 1973 and Manhes et al., 1978). Briefly, Pb was preconcentrated from 500 to 600 mL of acidified seawater by magnesium-hydroxide coprecipitation after ammonia addition in trace metal clean separatory funnels. The precipitate was collected by drawing off from the bottom of the funnel, concentrated into a pellet by centrifugation, and the supernatant siphoned off. The pellet was redissolved by the addition of trace metal clean 6 M HCl, and further concentrated by a second coprecipitation. After removing the supernatant, pellets were dissolved in 1.1 M HBr and Pb was separated from the sample matrix by anion column separation using a trace metal cleaned Eichrom AG-1 × 8 anion exchange resin. The concentrated sample was then evaporated to dryness until analysis. Prior to analysis, the samples were dissolved in 200–300 μL of 0.2 M trace metal clean HNO_3 and spiked with 1 ppb Tl to determine the mass fractionation factor (β). For each set of column separations, one or two column blanks were run. During analysis, ^{206}Pb/^{204}Pb (with 204 measurements on a Daly-style ion counter and 206 on a Faraday cup) was calibrated every five samples by bracketing with an internal laboratory standard "20% BAB3deg" (derived from a commercial Pb standard with an isotopic composition similar to typical U.S. Pb). On every analytical run, ^{206}Pb/^{207}Pb and ^{208}Pb/^{207}Pb Faraday cup measurements were bracketed at the beginning and end of each day with analyses of our internal lab standard "BAB3deg" and NBS-981. NBS-981 absolute values (Baker et al., 1987; Thirwall, 2000) were used to normalize each day's runs to compensate for small mass fractionation anomalies and Faraday cup efficiency differences. 0.2 M HNO_3 spiked with Tl blanks were run every 10 samples to drift-correct the hardware background signal, which derives mainly from previously-aspirated samples and standards. Hg was monitored at mass 202 to correct for any interference of ^{204}Hg on the ^{204}Pb signal. Masses 202, 203, 205, 206, 207, 208, and 210.5 were measured by the use of Faraday cups, while mass 204 was measured using a Daly-style ion counter. The Daly data were corrected for deadtime (from the slope of measured ^{206}Pb/^{204}Pb ratio vs. 204 count rate) and counting efficiency using an in-lab standard with a determined ^{206}Pb/^{204}Pb ratio ("20% BAB3deg"). We do not make use of the ^{206}Pb/^{204}Pb data here because it is linearly correlated with ^{206}Pb/^{207}Pb ratio within the scatter of our ion counting measurements.

Isotope ratio accuracy and precision have been estimated by 19 repeated analyses of an in-lab Pb standard relative to NBS-981 during the period when these samples were analyzed. ^{206}Pb/^{207}Pb of these analyses had a 2 standard deviation of 0.25‰ and ^{208}Pb/^{207}Pb had a 2 standard deviation of 0.19‰. These standards were run at the upper range of the concentration encountered for samples and it is expected that lower-concentration samples will have a higher uncertainty, although we expect that it only rarely exceeds 1‰ for either ratio.

2.4. Data management and repository

All Pb concentration data from this manuscript have been submitted to BCO-DMO and will be available at ⟨http://data.bco-dmo.org/jg/dir/BCO/GEOTRACES/NorthAtlanticTransect/⟩ and from the BODC International GEOTRACES Intermediate Data Product ⟨http://www.bodc.ac.uk/geotraces/data/idp2014/⟩. Pb isotope data will be deposited in BCO-DMO upon completion of standardization tests.

3. Results and discussion

The US GEOTRACES North Atlantic cruise track GA03 (Fig. 1) was chosen to optimally investigate as many processes and provinces within the constraints of an approximately zonal transect. It was completed in two sections, USGT10 from Portugal to the Cape Verde Islands, and USGT11 from Woods Hole, MA to the Cape Verde Islands. From west to east, the track transited from the seasonally productive New England coastal waters, to shelf and slope waters, crossing the deep western boundary current and the Gulf Stream along Line-W (Pickart, 1992; Schlitzer, 2007; Kuhlbrodt et al., 2007; Fine et al., 2002). After occupying the Bermuda Atlantic Time Series station (BATS), the track crossed through the oligotrophic Sargasso Sea, the North Atlantic Subtropical Gyre, the Mid-Atlantic Ridge hydrothermal TAG site, and over the northern reach of the tropical North Atlantic Oxygen Minimum Zone near the Cape Verde Islands and the Mauritanian Upwelling off the coast of Northwest Africa. The most eastward samples collected were along a meridional section from Portugal to the Mauritanian Upwelling, and sampled Mediterranean Outflow Water (MOW). From Optimum Multi-Paramater Analysis (Tomczak, 1981; Jenkins et al., 2015), other major water masses sampled included distal Antarctic Intermediate Water (AAIW), Upper Labrador Sea Water (ULSW), distal Antarctic Bottom Water (AABW), Upper Circumpolar Deep Water (UCDW), Atlantic Equatorial Water (AEW), Denmark Straights Overflow Water (DSOW), Iceland-Scotland Overflow Water (ISOW), Central Labrador Seawater (CLSW), Irminger Sea Water (ISW), North Atlantic Central Water (NACW), and Southwest Atlantic Central Water (SWACW).

3.1. Oceanographic section and basin distribution of dissolved Pb

High fluxes of anthropogenic Pb deposited into the North Atlantic Ocean during previous decades of alkyl leaded gasoline usage in the US and Europe have resulted in a present-day dissolved Pb maximum in thermocline waters that were ventilated during that period. Since the early 1980s, this maximum has been steadily decreasing and deepening (see Section 3.4) because of ventilation by younger waters that carry lower Pb concentrations from the surface as a result of the phaseout of leaded gasoline and also mixing with older pre-gasoline Pb waters and scavenging of Pb onto sinking particles. As a result of the time dependent changes in Pb fluxes to the ocean, and the subsequent incorporation of that Pb with ocean circulation, distinct horizontal and vertical gradients are observed across the basin (Figs. 1 and 2). The 2010–2011 Pb maximum occurs near the 27.0 sigma isopleth that is located at its deepest at BATS (~900 m), shallowing to ~500 m within the Mauritanian Upwelling, and shallowing to 300 m depth toward the Eastern end of the basin. This Pb maximum, where concentrations exceed 30 pmol/kg, is contained within ISW and ULSW, but is influenced notably by MOW along the Eastern Boundary (Jenkins et al., 2015).

Water within the western boundary feature (USGT10-01 to USGT10-10) is around 24–30 years old as determined by SF_6 age dating (see Section 3.4), which corresponds to the time period encompassing the phaseout of alkyl leaded gasoline. The waters above this feature are around 20–24 years old, and the lower Pb concentrations observed there are primarily contained within NACW.

On the eastern margin, MOW carries a high Pb signal and is dated by SF_6 to about 1974, that is similar in age to some of the deeper waters observed across the basin that have lower Pb concentrations. This could be because of the effect of water mass mixing on the calculated SF_6 age. The waters along the Eastern Margin are characterized by more than one end member and SF_6 age calculations do not represent the mean age if there are components older than about 30 years (Fine, 2011). Within the Mauritanian Upwelling, the Pb maximum occurs at a lower concentration than immediately to the west or north. Scavenging rates there may be higher as a result of elevated lithogenic particulate matter from the Sahara Desert, and elevated particulate organic matter because of the higher productivity of these waters (Lam et al., 2015). For these reasons, Pb may be scavenged more quickly here than along the western boundary. The impingement of AAIW at ~600 m depth along the Eastern Margin is also responsible for the lower concentrations observed at shallower depths. AAIW carries less Pb than ISW or ULSW because these waters outcrop in areas that are affected very differently by anthropogenic emissions. Emissions from the US and Europe may strongly influence the outcrops of ISW and ULSW at Northern latitudes, but there is much less of an impact by human activities on the waters forming around the Antarctic continent. Atlantic Equatorial Water (AEW) derived from 5–10°N, 20–40°W is a strong component of water on the eastern margin, and even though these waters are 10–30 years old by SF_6 age dating, the Pb concentration of equatorial surface waters is significantly lower than those north of ~20° (Helmers and van. der. Loeff, 1993; Boyle et al., 2014). The Eastern and Western parts of the basin are affected by different ventilation rates (Kuhlbrodt et al., 2007). The deeper penetration of elevated Pb concentrations along the western boundary is likely caused by transport of well ventilated ULSW and CLSW along the eastern continental slope of North America in the Deep Western Boundary Current and lateral exchange with older water in the interior, as evidenced by transient tracer measurements that indicate the deep penetration of waters that ventilated during times of higher atmospheric Pb deposition.

Deepwater differences between the two basins can be examined by comparing USGT11-12 to USGT11-20 which were located in the deepest portions of the Western and Eastern basins, respectively. The most distinct difference between the two is the contrast in concentration in intermediate waters between about 1000 m and 3000 m depth (Fig. 3A). As mentioned earlier, this difference is attributable to the differences in ventilation timescales and the areas that the dominant water masses occupy across the basin (Fig. 1B). A higher silicate concentration that tends to be characteristic of a contribution from AABW (Mantyla and Reid, 1983; Rutgers van der Loeff and van Bennekom, 1989) is observed in the deep waters in the western basin but there is little to no difference in the Pb concentration observed in the Western and Eastern basins below 5000 m in this 2011 data (Fig. 3A). The $^{206}Pb/^{207}Pb$ ratios show similar trends in deep water, with slightly elevated ratios and lower values in the deepest sample (Fig. 3B).

When plotted in triple isotope space (Grey and black dots, Fig. 3C), these deeper waters fall along a trajectory that is influenced by more than two end-members. The colored dots in Fig. 3C are historical Pb isotope data from surface coral cores from North Rock, Bermuda, whose Pb isotope values are close to seawater samples near BATS (Kelly et al., 2009). This plot puts the two stations in a temporal framework that highlights the pervasive anthropogenic influence of Pb on the seawater samples at all depths and the similarity of the surface water temporal evolution with the deepwater vertical variability (Fig. 3C). At USGT11-12 between 3500 and 5700 m, and at USGT11-20 between 3000 and 5400 m, there is a trend toward

slightly higher ratios with depth, followed by a decrease at the deepest depth (Fig. 3A and B). This trend is likely caused by the water masses occupying this depth range. The slightly lower concentration and $^{206}Pb/^{207}Pb$ ratios in the bottom water samples may also be a result of exchange with recently remobilized sediment containing anthropogenic Pb.

The deepest samples across the basin are between 7 and 10 pmol/kg (Figs. 1 and 2) with the exception of some samples along the eastern margin that are discussed in a later Section (3.9). The $^{206}Pb/^{207}Pb$ isotopic composition of pre-anthropogenic Pb has been determined in pelagic sediments and in Mn nodules in the North Atlantic to be between 1.207 and 1.212 (Chow and Patterson,

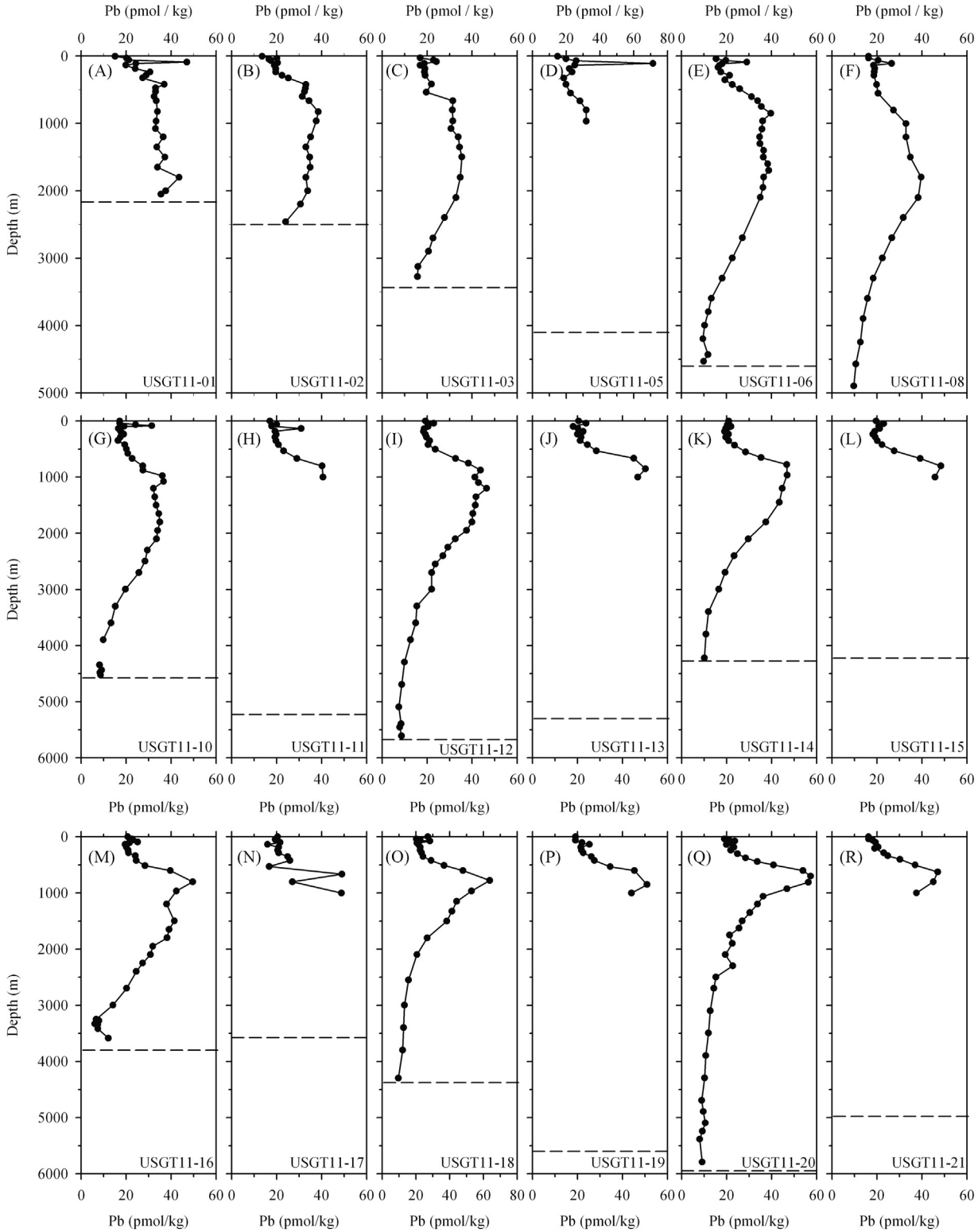

Fig. 2. Dissolved Pb profiles for the entire sampling effort. At most stations, intermediate waters carry a higher dissolved Pb feature because of the ventilation of anthropogenic Pb into NADW from atmospheric sources, but primarily emissions from alkyl leaded gasoline.

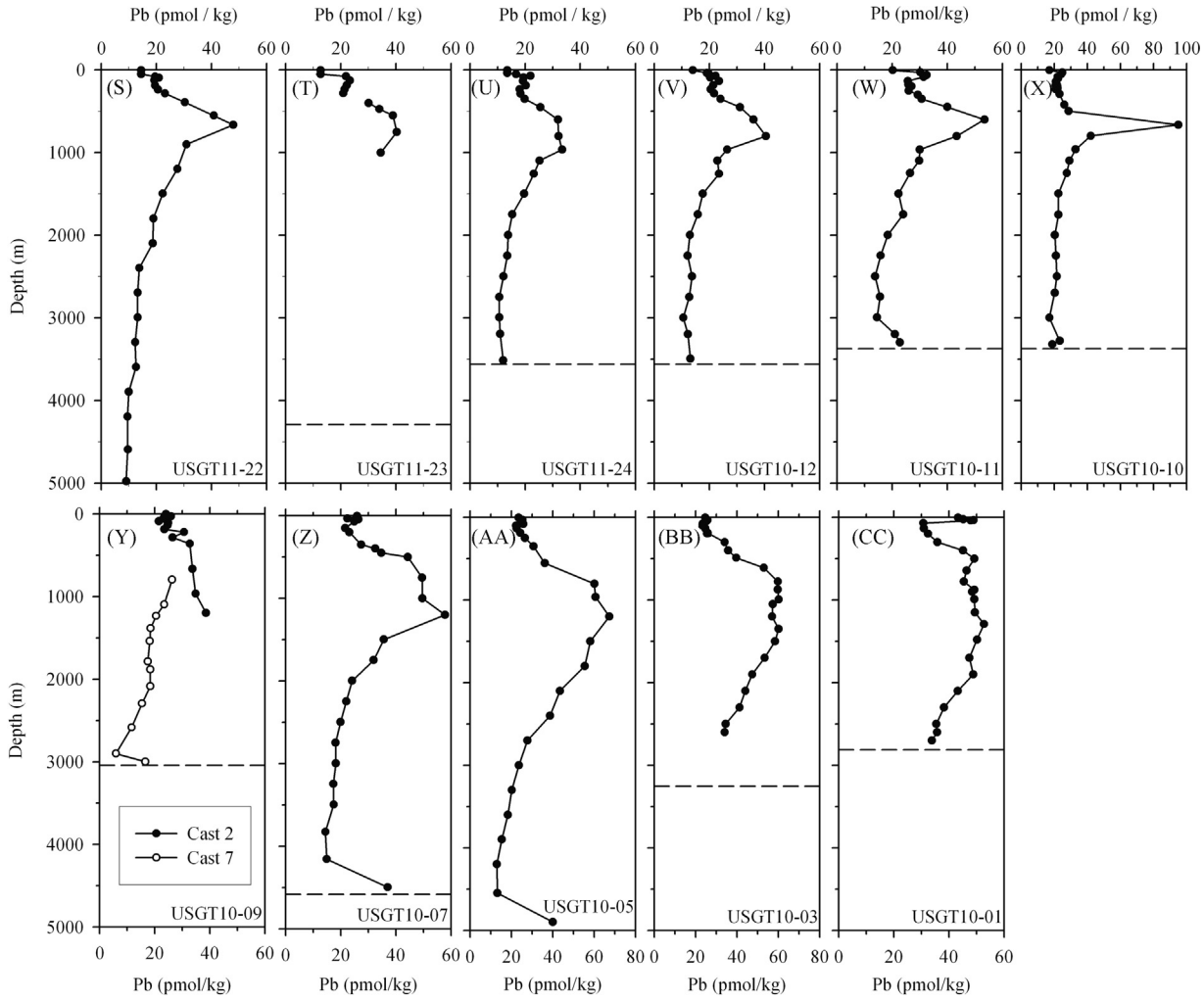

Fig. 2. (*continued*)

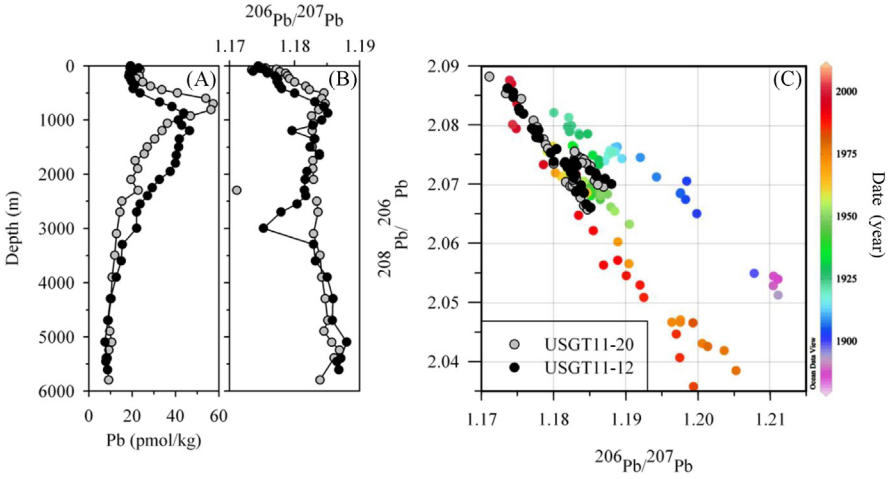

Fig. 3. (A) Pb concentration profiles for USGT11-12 (black) and USGT11-20 (grey). (B) Stable Pb isotope profiles showing the similarities and differences between USGT11-12 and USGT11-20 for $^{206}Pb/^{207}Pb$. (C) Triple isotope plot showing both stations compared to dated coral Pb isotope composition from Kelly et al. (2009).

1962), much higher than all the $^{206}Pb/^{207}Pb$ values observed by this study (Fig. 4). This observation of pervasive anthropogenic contamination is supported by previous observations of deep penetration of anthropogenic Pb even in the deep Pacific Ocean (Wu et al., 2009). Deep water is ventilated quickly along the western boundary by North Atlantic Deep Water, and the presence of CFCs throughout the water column suggests that ventilation alone is sufficient to explain the anthropogenic Pb signal observed

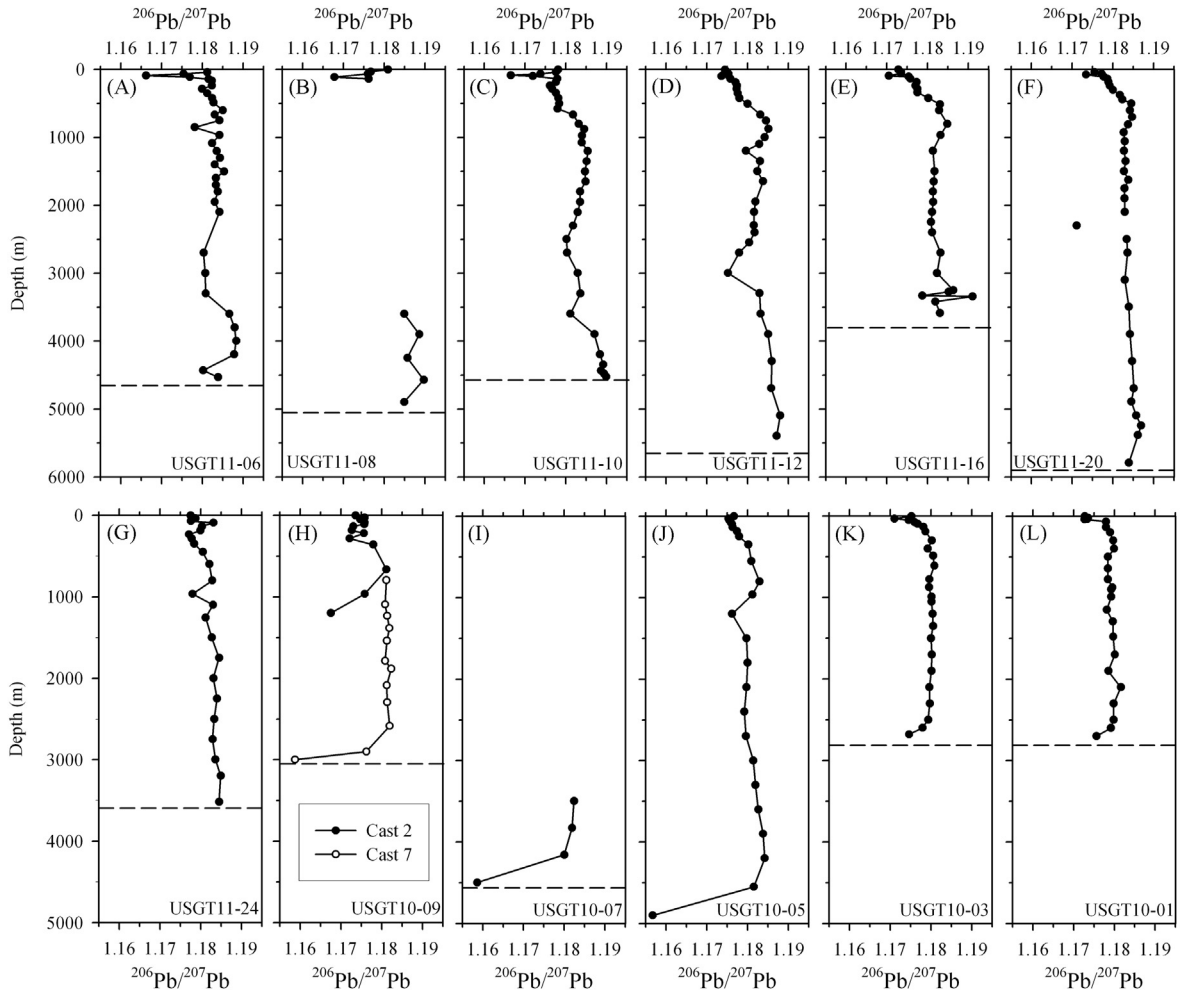

Fig. 4. Stable Pb isotope profiles showing $^{206}Pb/^{207}Pb$. Dashed lines indicate bottom depth.

in the deepest waters. CFCs have been entering the ocean for about 60 years while anthropogenic Pb has been entering the ocean for more than 100 years, therefore the detection of CFCs in deep waters necessarily implies an exposure to anthropogenic Pb (Fig. 4, Kelly et al., 2009). Another point to consider is that because particle transport from the surface is rapid (months), then Pb released from sinking particles should reflect the flux-weighted integral of the surface Pb isotope signal. In the deep Eastern Atlantic, it clearly does not, with isotope ratios similar to those at the surface during the 1920s and 1930s as opposed to the peak gasoline Pb years of the 1970s.

3.2. Evolving Mediterranean Outflow Water

Elevated Pb concentrations were observed within MOW. At USGT10-01, the concentration maximum was 48.9 ± 0.5 pmol/kg (n= 3, 875–990 m, 27.54–27.65σ_0), higher at USGT10-03 (59.9 ± 0.3 pmol/kg, n=3, 775–993 m, 27.44–27.67σ_0), and higher still at USGT10-05 (62.4 ± 4.4 pmol/kg, n=3, 962–1500 m, 27.54–27.83σ_0). The isotopic composition of these waters was fairly constant (USGT10-01: $^{206}Pb/^{207}Pb$= 1.1793 ± 0.0002, n=3; USGT10-03: $^{206}Pb/^{207}Pb$= 1.1797 ± 0.0003, n=3, USGT10-05: $^{206}Pb/^{207}Pb$= 1.1790 ± 0.0026, n=3). The depths at which the concentration maxima were located corresponded with a large percent contribution of MOW identified by temperature, salinity and nutrient tracers (Jenkins et al., 2015). Although no present day MOW depth Pb isotopic data currently exist from the Mediterranean, elevated concentrations in intermediate waters have been seen in samples collected from the Western Mediterranean in 1982, indicating that this basin could provide an intermediate depth source of elevated Pb to the North Atlantic (Moos and Boyle, in preparation), and other work also has demonstrated that this highly impacted basin is a major historical source of anthropogenic Pb (Laumond et al., 1984; Copin-Montegut et al., 1986; Lambert et al., 1991). A pure MOW Pb endmember concentration can be calculated by estimating a background salinity and Pb concentration for the Atlantic by visual interpolation of profile data, and using a salinity of pure Mediterranean Outflow Water from the literature of 38.45‰ (van Geen et al., 1988) to calculate contributions from the respective water masses assuming two endmember mixing. Using these values and assumptions and measurements of MOW properties at USGT10-01, MOW feeding into the Atlantic in 2010 would have had an estimated Pb concentration of 74 pmol/kg at USGT10-01 and a mean date of ventilation within the Mediterranean Sea determined by SF_6 to be about 1990. If these calculations are repeated at USGT10-03, the value of the MOW increases with distance from the Straight of Gibraltar to an endmember concentration of 150 pmol/kg, with an SF_6 ventilation date of about 1983. This change should be expected as a consequence of the temporal decrease in Pb concentrations within the Mediterranean Sea as Pb gasoline was phased out (Moos and Boyle, in preparation). The maximum may also be in part caused by mixing with the eastern North Atlantic Pb concentration maximum from 1970s ventilated water. MOW within the Mediterranean Sea has a short residence time on the order of ~100 y (Lacombe et al., 1981) and the isotopic composition is fairly constant within the depth range that defines this water mass

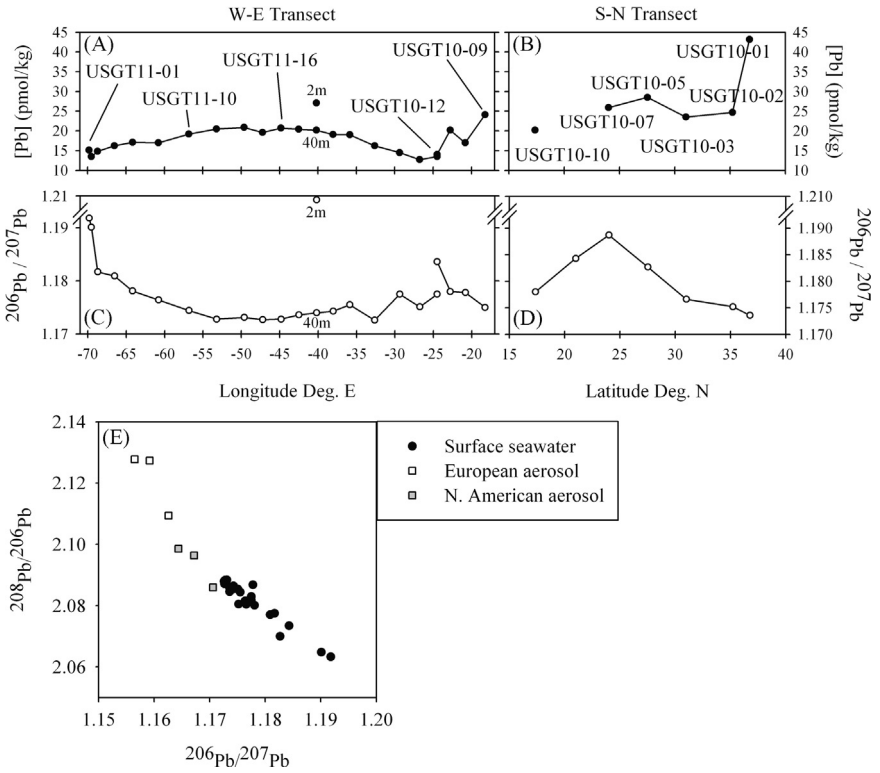

Fig. 5. Surface transect data for (A) Pb concentrations across the zonal transect, (B) Pb concentrations along the meridional transect, (C) $^{206}Pb/^{207}Pb$ isotope ratios across the zonal transect, and (D) $^{206}Pb/^{207}Pb$ isotopic ratios along the eastern meridional transect. Note that the "fish" surface sample at 40°E is very different from the 40 m GTC sample that was at the base of the mixed layer. We suspect that this "fish" sample is contaminated and that the 40 m GTC sample is representative of the true mixed layer composition. (E) Shows a comparison in triple isotope space between surface samples and collected aerosol data.

coming from a relatively well-mixed reservoir. Surface concentrations in the northern Mediterranean were in excess of 500 pmol/kg in 1980, but have decreased with time (Moos and Boyle, in preparation). Across both expeditions, Stations USGT10-03, USGT10-05, and USGT11-20 showed the most elevated concentrations at their intermediate depth maxima (Fig. 2). At USGT10-05 and USGT11-20, the complex mixing hydrography negates the simplified MOW salinity endmember estimation calculations, although the Pb maxima (67 and 57 pmol/kg, respectively) were comprised of approximately 50% and 30% primary MOW, respectively.

3.3. Surface distributions of Pb and Pb isotopes

Across the basin, surface concentrations and isotopes reflect recent fluxes to the surface ocean, and give an indication of the source region of those fluxes. Surface concentrations across the 2011 near-zonal transect generally fell below 21 pmol/kg (Fig. 5). This value is significantly lower than has been observed in previous decades when surface concentrations in the Atlantic exceeded 150 pmol/kg (Schaule and Patterson, 1981; Kelly et al., 2009). Isotope ratios show a decrease in $^{206}Pb/^{207}Pb$ ratios toward the Eastern margin (Fig. 5). This decrease is caused by an increase in the relative inputs of European-derived Pb relative to US-derived Pb. Historically, aerosols borne by the Easterlies and Trade Winds exhibited low $^{206}Pb/^{207}Pb$ isotope ratios (Hamelin et al., 1997). Aerosols from Western Europe in the late 1980s generally showed lower values (1.116–1.155: Hopper et al., 1991; Véron et al., 1994) than West African and Mediterranean aerosols (1.147–1.167: Véron et al., 1993; Véron and Church, 1997; Church et al., 1990). Aerosols from the Westerlies have historically exhibited higher $^{206}Pb/^{207}Pb$ isotope ratios (Alleman et al., 2001a), with values in the late 1980s that were collected from Eastern USA source regions that were much higher (1.198–1.210: Véron et al., 1992; Church et al., 1990). Aerosol studies in the late 1980s and early 1990s have demonstrated a range in these ratios (Véron et al., 1994), and highlight the complexity of pinpointing one source. The observed trend in the surface transect toward lower $^{206}Pb/^{207}Pb$ ratios in the southeast is largely a result of the earlier completion of leaded gasoline phase-out by the US, thus increasing the fractional contribution of low isotope ratio Pb from European and North African emissions (Véron et al., 1998; Wu and Boyle, 1997; Erel et al., 2006).

In the meridional stations from the USGT10 transect, concentrations are higher in surface waters, ranging from 23 to 43 pmol/kg (Fig. 5B). $^{206}Pb/^{207}Pb$ ratios decrease as stations approach Portugal, reaching the lowest surface $^{206}Pb/^{207}Pb$ ratio of 1.173 at Station USGT10-01 (Fig. 5B). Surface concentrations are lowest approaching the Western margin (13.5 pmol/kg at USGT11-02) and in the middle of the Eastern Basin (12.7 pmol/kg at USGT11-23). Off the coast of Mauritania, the concentrations increase with proximity to the coast, presumably caused by anthropogenically-contaminated dust from North Africa. Samples were also collected for aerosols, and the isotopic composition of 6 aerosol samples are shown in a triple isotope plot along with the surface samples in Fig. 5E. Interestingly, the modern North American end member aerosol, identified by wind direction and sampling location, has a low $^{206}Pb/^{207}Pb$ isotope ratio relative to historical values (Véron et al., 1992; Church et al., 1990; Alleman et al., 2001a, 2001b). This decrease may reflect the growing relative importance of non-leaded gasoline anthropogenic inputs from North America that include high temperature industrial processes, coal burning and smelting. These processes may use a source ore that is characterized by a different Pb isotope composition than those that were used in the US during these earlier samplings. Some work in Canada has also suggested that aerosols and snow in that region are characterized by much lower $^{206}Pb/^{207}Pb$ isotope ratios (~1.15) than that of Mississippi River Valley Pb that was

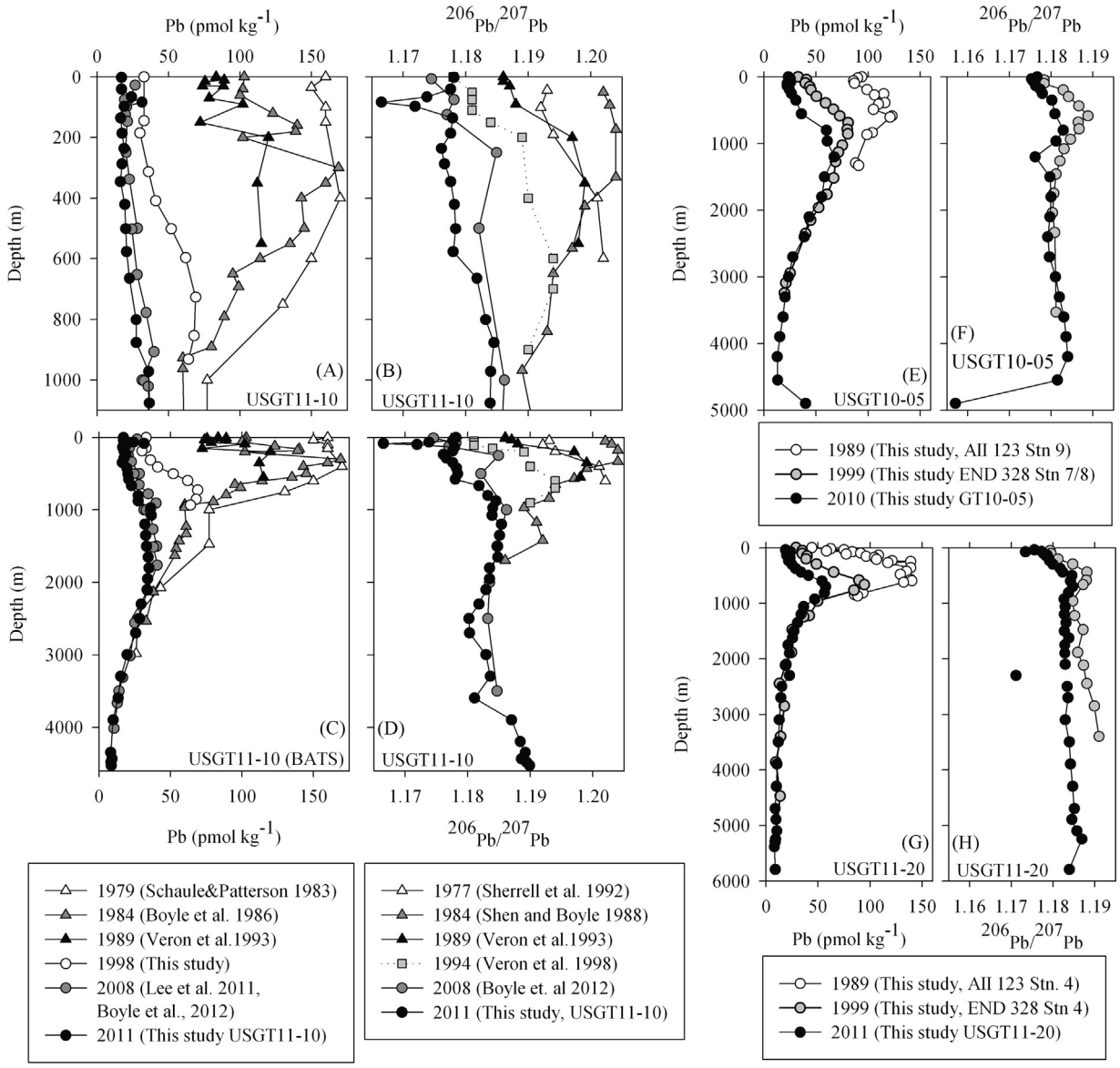

Fig. 6. Time series profiles showing (A and B) Pb concentration and isotopic composition in the upper 1000 m nearby BATS and (C and D) full depth during the past 32 years. Two other stations have been occupied previously by our lab and time series (E) Pb concentration data and (F) isotopic data are shown for USGT10-05 during the past 21 years as well as (G) Pb concentration data and (H) isotopic composition for USGT11-20 during the past 22 years.

responsible for much of the American-derived Pb emissions for some time (Simonetti et al., 2000a, 2000b, 2003; Shotyk et al., 2005). If Canadian aerosols are becoming a more important contributor to anthropogenic Pb in the Westerlies, this increasing source could explain the shift in isotopic composition observed relative to aerosols collected in the 1980s that were characterized by much higher $^{206}Pb/^{207}Pb$ isotope ratios that hovered around 1.21 (Véron et al., 1992; Church et al., 1990).

3.4. *Temporal evolution of Pb in the North Atlantic at three stations during the past 30 years*

For three Stations (USGT10-05, USGT11-10, USGT11-20), water column data exist that span the last 2–3 decades (Fig. 6, Table 1). Beginning with the first Pb profile from 1979 samples near Bermuda published by Schaule and Patterson (1983), concentrations have decreased dramatically over time down to at least 2500 m from a maximum of 170 pmol/kg to a present day maximum of 36 pmol/kg (Fig. 6A and C). This trend holds true for the two time series occupations in the Eastern basin as well near USGT10-05 and at USGT11-20 (Fig. 6E and G).

There has also been a temporal shift in the Pb isotope signatures (Fig. 6B, D, F, H). During earlier decades, $^{206}Pb/^{207}Pb$ ratios were dominated by US derived Pb, with values trending more toward a US end-member in excess of 1.20 (Hamelin et al., 1997; Shen and Boyle, 1988; Weiss et al., 2003). Over time, that ratio has decreased, reflecting both an increasing relative influence of lower $^{206}Pb/^{207}Pb$ European-derived Pb, and a decrease in fluxes from US sources created by the phase out of leaded gasoline (1984–1998). In more recent years, however, it appears that the ratios may be increasing again, at least in surface waters at BATS, toward a more even balance between the US and European fluxes from industrial processes now that leaded gasoline derived fluxes of Pb to the Atlantic from both the US and Europe have been completely phased out. It is also worth noting that the deeper Eastern Atlantic waters also show lower $^{206}Pb/^{207}Pb$ in 2011 compared to 1999 down to at least 3200 m (Fig. 6H). The Pb isotopic composition ($^{206}Pb/^{207}Pb$ and $^{208}Pb/^{207}Pb$) of the 1999

Table 1
Dissolved Pb data for previously unpublished occupations of USGT10-05, USGT11-10, and USGT11-20 in the first, second, and third columns, respectively.

Depth (m)	Pb (pmol/kg)	^{206}Pb	^{207}Pb	Depth (m)	Pb (pmol/kg)	^{206}Pb	^{207}Pb	Depth (m)	Pb (pmol/kg)	^{206}Pb	^{207}Pb
		^{207}Pb	^{208}Pb			^{207}Pb	^{208}Pb			^{207}Pb	^{208}Pb
2011 (USGT11-10)				2010 (USGT10-05)				2011 (USGT11-20)			
2	17.1	1.1781	2.4506	2	23.5	1.1766	2.4479	41	19	1.1755	2.4503
40	17.1	1.1776	2.4495	30.7	25.3	1.1753	2.4469	66	21.3	1.1772	2.4495
66	24.2	1.1738	2.4462	51.5	24.7	1.1755	2.4481	76	23.6	1.1734	2.4470
84	31.4	1.1665	2.4413	80.9	25.7	1.1759	2.4481	106	21.4	1.1777	2.4492
97	19.1	1.1719	2.4443	101.3	22.3	1.1762	2.4485	137	19.9	1.1786	2.4486
135	16.5	1.1779	2.4490	135.6	22.5	1.1763	2.4480	187	23.2	1.1789	2.4481
186	17.6	1.1776	2.4487	186.8	24.3	1.1774	2.4483	236	21.8	1.1792	2.4480
236	18.9	1.1761	2.4483	251.1	26.5	1.1779	2.4478	301	24.8	1.1800	2.4466
287	17.4	1.1766	2.4484	350.6	30.7	1.1802	2.4480	376	28.4	1.1817	2.4465
346	16.4	1.1776	2.4498	553	36.1	1.1809	2.4483	441	33.6	1.1823	2.4470
421	19.4	1.1782	2.4509	802.1	60.1	1.1829	2.4491	501	40.8	1.1845	2.4472
502	20.1	1.1784	2.4476	962.8	60.7	1.1812	2.4488	601	53.9	1.1842	2.4469
577	20.7	1.1780	2.4484	1201.8	67.4	1.1762	2.4477	700	57.3	1.1847	2.4471
665	22.7	1.1818	2.4478	1500.9	58.2	1.1797	2.4502	810	56.3	1.1837	2.4476
801	27.4	1.1832	2.4478	1800.3	55.5	1.1800	2.4502	926	46.8	1.1826	2.4477
876	27.5	1.1845	2.4500	2100.3	43.5	1.1797	2.4508	1061	36.2	1.1829	2.4489
972	36.1	1.1840	2.4499	2400.8	38.7	1.1792	2.4513	1199	33.7	1.1827	2.4490
1076	36.6	1.1839	2.4511	2700.6	27.7	1.1796	2.4523	1349	30.3	1.1831	2.4501
1201	32.1	1.1854	2.4529	3000.6	23.6	1.1810	2.4502	1500	26.9	1.1827	2.4512
1352	32.7	1.1851	2.4532	3301	20.2	1.1820	2.4509	1626	25.5	1.1838	2.4500
1501	33.3	1.1847	2.4526	3600.1	18.3	1.1830	2.4517	1750	21.3	1.1828	2.4523
1651	34.5	1.1848	2.4520	3899.2	15.3	1.1836	2.4530	1897	22.5	1.1828	2.4523
1800	35	1.1835	2.4528	4199.1	12.9	1.1840	2.4535	2099	19.4	1.1829	2.4535
1951	34	1.1835	2.4514	4548.7	13.2	1.1815	2.4514	2298	22.7	1.1711	2.4454
2101	33.5	1.1829	2.4510	4898.6	40	1.1570	2.4356	2497	15.2	1.1834	2.4550
2299	29.4	1.1818	2.4506					2698	14.3	1.1836	2.4551
2498	28.4	1.1802	2.4498	1999 (Stn 7, END328)				3096	12.7	1.1829	2.4550
2698	25.7	1.1803	2.4497	47		1.1783	2.4452	3496	11.9	1.1839	2.4559
2998	19.7	1.1829	2.4517	98		1.1783	2.4458	3896	10.7	1.1842	2.4561
3298	15.2	1.1836	2.4526	98		1.1783	2.4445	4295	10.2	1.1847	2.4563
3597	13.3	1.1811	2.4536	197		1.1829	2.4455	4696	8.9	1.1851	2.4566
3897	9.8	1.1870	2.4583	295		1.1842	2.4471	4892	9.6	1.1845	2.4559
4196	n.a.	1.1884	2.4605	436		1.1866	2.4483	5096	10.5	1.1857	2.4551
4346	8.2	1.1892	2.4611	586		1.1888	2.4493	5243	9.2	1.1869	2.4562
4436	9.1	1.1886	2.4598	680		1.1865	2.4468	5384	8	n.d.	n.d.
4479	8.3	1.1894	2.4613	782		1.1867	2.4478	5792	9.1	1.1839	2.4549
4526	8.6	1.1899	2.4615	937		1.1846	2.4492				
				1078		1.1831	2.45	1999 (Stn 4, END328)			
2008 (USGT08)				1261		1.1821	2.4507	0.5	28.8		
7		1.1745	2.4455	1458		1.1812	2.4505	56	35	1.1793	2.4469
75		1.1781	2.4478	1745		1.1806	2.4501	102	34.9	1.1795	2.4478
125		1.1770	2.4486	2037.6		1.1803	2.4506	151	39.5	1.1784	2.4456
250		1.1849	2.4529	2337		1.1808	2.4518	201	38.5	1.1812	2.4461
500		1.1821	2.448	3528		1.1812	2.4532	296	48.5	1.1847	2.446
1000		1.1862	2.4529					438	65	1.1881	2.4484
1500		1.1848	2.4524	1999 (Stn 8, END328)				584	89.4	1.1880	2.4481
2000		1.1835	2.4494	0.5	32.8			664	94.4	1.1872	2.4478
2500		1.1832	2.4519	40	40.8			765	84.6		
3500		1.1847	2.4534	94	39.8			957	49.5	1.1847	2.4485
				146	44.1			1222	41.7	1.1852	2.4527
				195	45.2			1244	36.2		
				294	50.3			1473	25.4	1.1872	2.4582
				390	59.1			1886	24.4	1.1859	2.4581

2008 (Lee et al., 2011; USGT08)	
27	26.6
74	22
75	19.2
98	20.7
125	19.9
147	21.2
243	19.9
250	20.4
338	22.6
500	28.2
503	24.4
653	28.1
778	34.4
907	39.8
1000	31.6
1003	32.9
1021	35.9
1268	37.7
1500	40.3
1515	38.1
1762	40.7
2107	33.9
2500	27.9
2559	25.1
3011	21.7
3312	16.5
3500	13.9
3662	12.9
4014	10.6

1998 (winter)	
0	33
145	33
185	30
313	36
409	41
502	52
597	62
727	69
854	68
932	64

1999 (Stn 8, END328)	
485	66.7
586	72.9
687	80.7
787	80
856	80.6
1025	75.2
1130	71.4
1273	68.7
1518	67
1764	60.5
1960	52.5
2152	44.9
2352	40
2943	25.2
3091	21.1
3242	19.8

1989 (AII 123 Stn. 9, 35N, 29W)	
0	94
19	90
58	86
97	87
194	99
253	115
272	106
389	116
409	110
488	105
587	123
607	121
836	104
865	99
1294	88
1328	91

1999 (Stn 4, END328)			
2117	18.8	1.1873	2.4614
2442	13.1	1.1881	2.4617
2848	17.7	1.1899	2.4599
3396	14.1	1.1910	2.4654
3858	9.5		
4472	13.6		
5293	8.9		

1989 (AII 123 Stn. 4)	
0	44
19	62
39	75
58	58
77	83
97	91
116	77
135	108
154	96
174	104
212	106
232	121
251	139
270	117
361	139
425	135
477	129
574	139
594	140
622	132
815	93
844	85
872	88

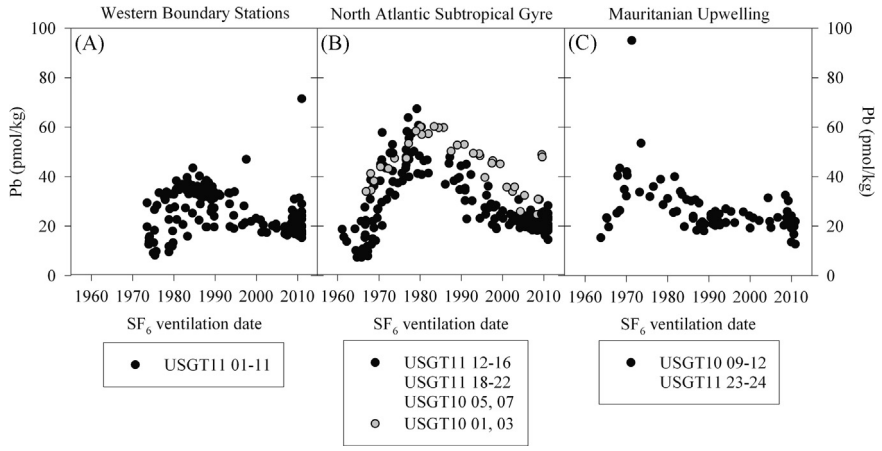

Fig. 7. SF_6 age dates versus Pb for (A) western boundary stations, (B) North Atlantic Subtropical Gyre, (C) Mauritanian Upwelling.

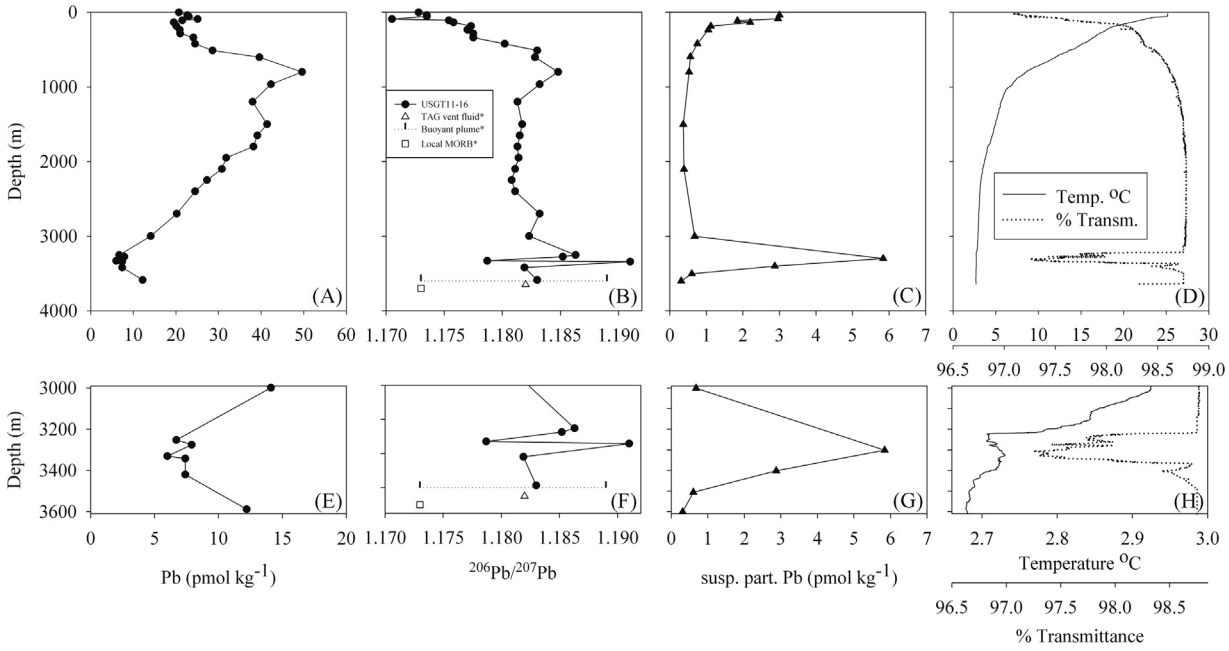

Fig. 8. Full depth profiles at the TAG Hydrothermal field site. (A) Pb concentration, (B) Pb isotope composition, (C) suspended particulate Pb, (D) and temperature and beam transmittance. A zoomed in view of the above properties within the hydrothermal plume is shown in E, F, G, and H. *Values from Godfrey et al., 1994.

Eastern Atlantic deep waters is the same as Bermuda surface corals show for 1915 (Fig. 3C), implying an ~85 year transit time for Pb from the surface Atlantic to the deep eastern basin. The Bermuda corals also show a $^{206}Pb/^{207}Pb$ drop from 1.19 to 1.18 in 1925, similar to the deep eastern basin seawater change during the 12 years between our 1999 and 2011 station occupations (Figs. 3C, 6D, F, H).

Another way to look at the temporal evolution of Pb is to compare the Pb concentration data to the corresponding SF_6 ages (Fig. 7). In general the data fall into three similarly shaped groups: the western boundary Stations (Fig. 7A), North Atlantic Subtropical Gyre (Fig. 7B), and the Mauritanian Upwelling (Fig. 7C). In the gyre and Mauritanian Upwelling, the Pb maxima are generally observed at the time of peak Pb usage between the mid 1970s and 1980s, though it is interesting to see that the stations most intensely affected by MOW have a slightly different shape than the surrounding waters, with slightly higher concentrations persisting into more recent decades (Fig. 7B). The western boundary stations show a different trend, with lower concentrations and more recent SF_6 ages (Fig. 7A). This feature of the western boundary Pb concentrations results from the more intense current systems and possibly from increased scavenging along the western boundary path. The two samples showing elevated concentrations in the western boundary waters that have young SF_6 ages are a result of samples from STUW, discussed below in Section 3.6. The samples observed to have higher concentrations with younger ages in Mediterranean Outflow waters are caused by anthropogenic surface input at USGT10-01, that was the closest station to Lisbon (Fig. 2CC).

3.5. *Pb concentration and isotopic signatures at the TAG hydrothermal field*

During the occupation of USGT11-16 (26.14°N–44.83°E, Fig. 1), located above the Mid-Atlantic Ridge, five samples were taken within the TAG hydrothermal plume. All five samples have Pb concentrations of 7.1 ± 0.8 pmol/kg, ~6.1 pmol/kg lower than the samples immediately above and below the plume (12.1 and 14.1 pmol/kg) (Fig. 8). This data (and the particulate data discussed below) suggests that the TAG hydrothermal system acts as a net sink for Pb from the water column, and that the enriched Pb in the hydrothermal emanations is completely precipitated and removed

to the underlying sediments without spending much time in the water column in dissolved or particulate form. Hydrothermal sediments at this site contain basaltic Pb, although the isotopic signature of basaltic Pb and Pb in the buoyant plume span a fairly large range (Fig. 8A and E, Godfrey et al., 1994). The variable isotopic signature observed in the seawater samples within the plume makes it hard to clearly identify a basaltic signature (Fig. 8B and F), but even if there is some basaltic contribution, on the whole there is net removal of Pb from the water column.

Samples for sinking and particulate metals were collected inside and outside the plume (Ohnemus and Lam, 2015). Pb concentrations in the suspended particles show a maximum in the plume of 8.6 pmol/L compared to surrounding suspended particulate Pb concentrations of <2 pmol/L (Fig. 8C and G). Compared to the average of the suspended particles below and above the plume, this particulate pb constitutes a 7.3 pmol/L excess, that is within analytical error of the 6.1 pmol/kg missing from the dissolved pool. Hence the observed excess in the particulate phase accounts for the deficit in the dissolved pool. It appears that there is no trace of hydrothermal Pb in the neutrally buoyant plume, and that Pb emitted by the hydrothermal activity is rapidly precipitated and is not carried upward into the neutrally buoyant TAG plume.

3.6. Subtropical underwater carries a European isotopic signature

Between USGT11-01 and USGT11-18, shallow Pb maxima are observed intermittently at some stations between 90 and 150 m, coincident with low $^{206}Pb/^{207}Pb$ isotope excursions (Fig. 9). These maxima coincide with the depth range expected for Subtropical Underwater (STUW) that forms in the North Atlantic Gyre and is identified by a subsurface salinity maximum (O'Connor et al., 2005). This salinity maximum is observed in many of the profiles that show Pb maxima coincident with $^{206}Pb/^{207}Pb$ minima, although the salinity maxima are not always coincident with the depth or density of the Pb features (Fig. 9). The salinity and Pb features do not have to be observed at coincident depths, however, because salinity is a near steady state tracer, while Pb concentrations and isotopes are evolving dramatically over time (order of magnitude decrease during the past 30 years). As such, the salinity and Pb features are related, even if their maxima are not coincident. During formation of STUW, warm but salty (and hence denser) water is subducted. The North Atlantic has the fastest subduction rate of the 4 global STUW masses (North Atlantic, North Pacific, South Pacific, South Indian), and is driven by vertical pumping (O'Connor et al., 2005). From CFC data and drifter data, the highest subduction rates for STUW are estimated to exist between USGT11-13 and USGT11-15, and have an average age of 1–5 years (O'Connor et al., 2005). USGT11-13, 14, and 15 sampled the lowest surface isotope ratios of both cruises ($^{206}Pb/^{207}Pb = 1.1727$, 1.1740, and 1.1728, respectively), with the exception of USGT10-01 and USGT10-02, that were proximate to Lisbon, Portugal (Fig. 5). Although these mid-Atlantic stations are remote, aerosols travel great distances and recent work has demonstrated transatlantic transport of African derived aerosols all the way to the Caribbean (Kumar et al., 2014). The low surface water $^{206}Pb/^{207}Pb$ ratios observed in the central North Atlantic Gyre are likely derived from anthropogenic European or North African sources. In the study by Weiss et al. (2003), European trade winds carried a $^{206}Pb/^{207}Pb$ signal around 1.142, compared to the African trade winds at 1.155. Both these signals are much lower than the overall average 1.18 signal observed in much of the upper water column across the Atlantic, and either could contribute to the low isotope excursions. With potential pollution of African-derived dust from European source as well, and the evolution of these signatures

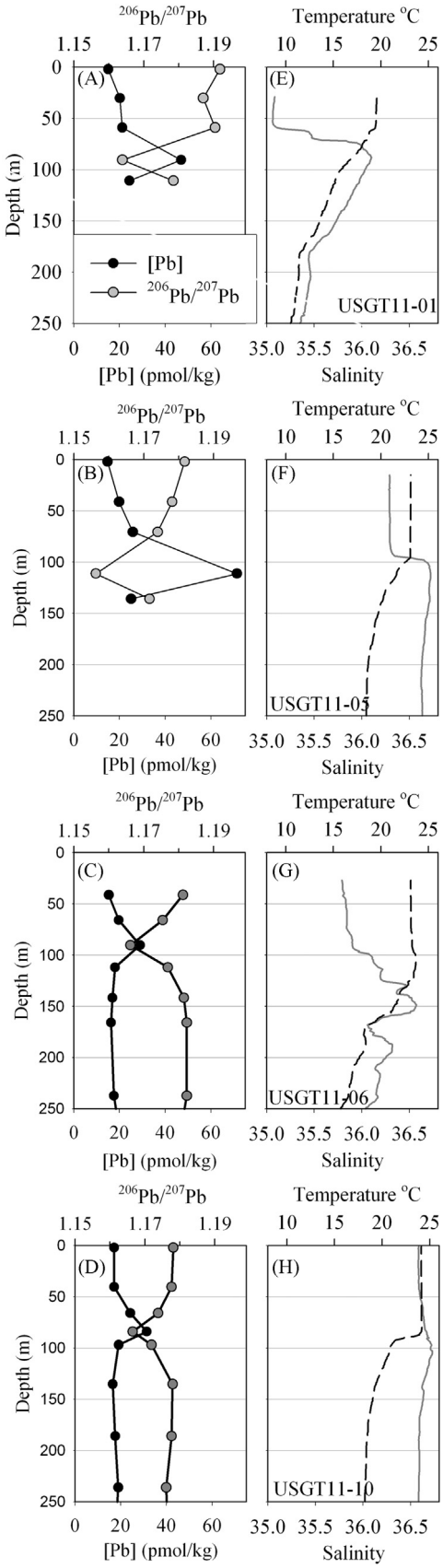

Fig. 9. Shallow profiles of dissolved Pb and $^{206}Pb/^{207}Pb$ ratios show the most prominent evidence of STUW at (A) USGT11-01, (B) USGT11-05, (C) USGT11-06, and (D) USGT11-10. These are complimented by features observed in the continuous CTD temperature and salinity data (E, F, G, H).

over time, it is difficult to pinpoint an African over a European source. However, Erel et al. (2006, 2007) has shown that modern African dust has been contaminated by anthropogenic lead from Europe and Northern Africa, reflecting a mixture between that and pre-anthropogenic dust with higher $^{206}Pb/^{207}Pb$ ratios (Erel et al., 2006, 2007).

The surface water Pb concentrations and isotope trends in the region of STUW origin appear to be fairly smooth, therefore we suspect that the apparent patchiness of the observed subsurface Pb and Pb isotope features may be in part a result of coarse Pb vertical resolution of STUW rather than caused by patchy existence of the feature. In addition, the CTD vertical profiles for salinity – that do not suffer the problem of limited resolution – shows that the strength of the subsurface salinity maximum is highly variable with a similar degree of patchiness (e.g., there is only a slight salinity maximum at USGT11-13 but quite a strong one at USGT11-14, Fig. 1). The strongest Pb and Pb isotope signals were seen at USGT11-05, a station along Line-W. The isotopic signature observed along with the concentration feature is supported by adjacent samples (forming a "tail" to the feature). Fig. 10 shows the mixing diagram, where the inverse of the Pb concentration is plotted against the $^{206}Pb/^{207}Pb$ isotope signature. The observed linear trend is suggestive of two end-member mixing, though teasing apart the exact sources is difficult and it may be possible that more than two sources could lie along this line. SF_6 data suggest that waters occupying this shallow feature are relatively young, and the end members are likely generated from differing modern sources. This shallow signal observed in STUW is evidence illustrating the importance of high-resolution studies like GEOTRACES. Without high vertical and lateral resolution of the upper water column, this feature may have been missed entirely, or even if sampled, likely dismissed as isolated contaminated samples, if only observed at one depth or at one station (n.b.—the International GEOTRACES Standards and Intercalibration Committee initially dismissed the USGT11-10 STUW Pb maximum as a "flyer").

3.7. Western boundary isotope signatures

Concentrations within intermediate waters along the western boundary fall consistently below 40 pmol/kg (Fig. 2). The isotopic composition of deeper waters at USGT11-06, USGT11-08 and USGT11-10 show evidence of two water masses that contain distinct isotopic features between 2500 and 4250 m depth (Fig. 4A–C). As defined by OMPA analysis, the western boundary of the North Atlantic is characterized by ULSW, CLSW, ISOW, DSOW, and AABW (Jenkins et al., 2015). It appears that two water masses are imprinted with different Pb isotopic composition, at the times that these waters ventilated. This difference is a result of temporal and spatial differences in the locations of the outcropping of these waters, the origin of the Pb deposited to the surface waters when they ventilated, and the respective timescales of ventilation of either water mass. For example, lower $^{206}Pb/^{207}Pb$ ratios observed in ISOW have been attributed to influences from European sources (Véron et al., 1999; Weiss et al., 2003) and likely explain some of this shift. The shifts in isotopic composition fall along changes in the major percentage of different water masses most distinctively at USGT10-06 (Fig. 11B, Jenkins et al., 2015). At 2700–3300 m depth, a $^{206}Pb/^{207}Pb$ ratio of 1.1805 appears to be associated with a higher percentage influence of ISOW, and at 3600–4200 m depth, the $^{206}Pb/^{207}Pb$ ratios of 1.185 appears to correspond with a higher percentage of DSOW. In the bottom sample, the ratio varies, and may be somewhat influenced by the thick nepheloid layer here that extended ~100 m up from the bottom.

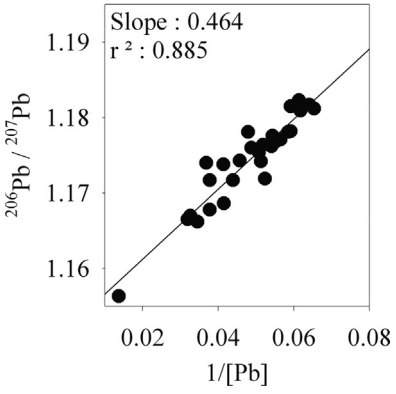

Fig. 10. Upper water column mixing diagram suggesting a mixing of two end members in the surface waters between USGT11-03 and USGT11-11.

In addition to the dissolved data, six samples were analyzed for the isotopic composition of the suspended particles (Fig. 11B and G) to examine the possibility of reversible exchange on particles. Previous work suggested that isotopic equilibrium was observed between suspended particles and surrounding seawater near Bermuda (Sherrell et al., 1992). Identical dissolved and particulate Pb isotope ratios were not observed in some samples from our new measurements, although the time between sampling of dissolved Pb isotope and particulate Pb isotopes in this dynamic region makes it possible that this apparent disequilibrium is misleading. Some exchange of Pb with particles and reversible scavenging may occur, similar to that observed for Th isotopes (Bacon and Anderson, 1982), and this issue requires further study.

3.8. Reoccupation of station TENATSO and observations at USGT10-09: Short term changes in intermediate waters

Time series Station TENATSO (Tropical Eastern North Atlantic Time Series Observatory) was occupied twice, at the end of each expedition (USGT10-12 and USGT11-24). This unique opportunity shows the temporal change between the sampling on November 2, 2010 (USGT10-12) and December 10, 2011 (USGT11-24). Although the observation of differences in the shallow waters are not surprising given previous reports of significant temporal variability in surface Pb concentrations (Boyle et al., 1986), there is some surprise in observing differences in deeper thermocline Pb concentrations (Fig. 12). For further comparison, a profile sampled at this location in August 2008 is also shown (cruise OCE449-2). This profile has a similar shape in thermocline waters to the profile from 2011, though with slightly elevated concentrations (Fig. 12).

In addition to these offsets observed after 1–3 years, a significant offset was observed between two casts at the same station closer to the Mauritanian margin (USGT10-09 Figs. 2Y, 4H). These two casts were taken 16 h apart (Cast 2: October 27, 21:20; Cast 7: October 28, 13:27) and showed a dramatic difference in both concentration and isotopic composition (Figs. 2Y, 4H). This observation indicates even faster changes in intermediate water Pb in the coastal region, and this phenomenon has not been previously observed. USGT10-09 sampled waters that are affected by fairly complex hydrography at intermediate depths (Stramma and Schott, 1999; Stramma et al., 2005). This offset between casts is observed between 800 and 1235 m depth. AAIW and UCDW both occupy water between 500 and 1200 m depth, and flow fields suggest that the cruise may have crossed part of a northern flowing arm of weakly cyclonic circulating AAIW at USGT10-09 (Stramma and Schott, 1999). There has been some debate about the direction of this flow, and the complexity of water masses in this region could lead to the variability observed between the two casts. Cast 10 at this station shows distinct water masses at 800 and 1200 m depth (Jenkins et al., 2015). The 800 m sample was comprised of mostly AAIW and MOW, whereas at 1200 m depth there was no AAIW and instead this depth was

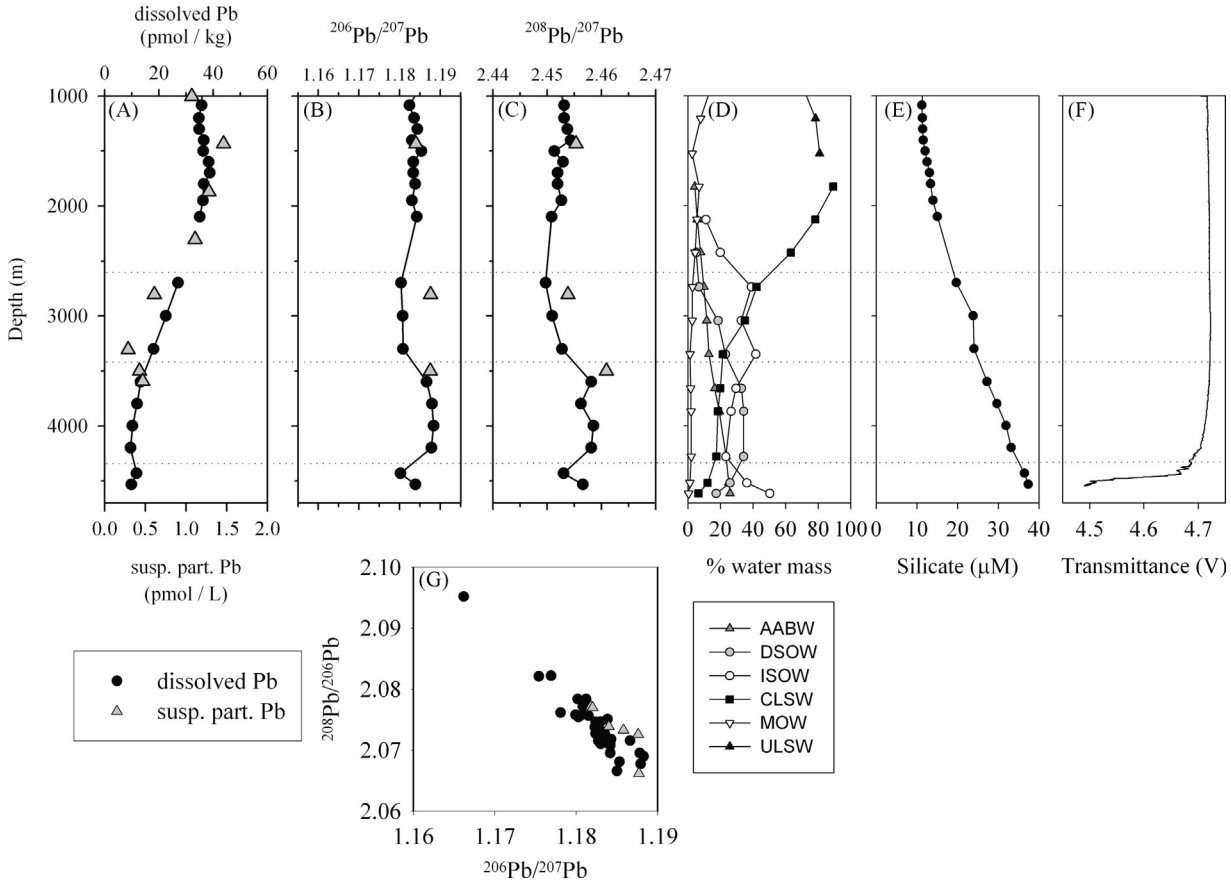

Fig. 11. Profiles for USGT11-06 of dissolved and suspended particulate (A) concentration (B) $^{206}Pb/^{207}Pb$ ratios, (C) $^{208}Pb/^{207}Pb$ ratios. The accompanying (D) water mass composition, (E) silicate concentration, and (F) transmittance can help identify features that help explain trends in the isotopic composition. (G) Triple isotope plot of dissolved and suspended particulate Pb at USGT11-06. Dashed horizontal lines denote changes in significant water masses.

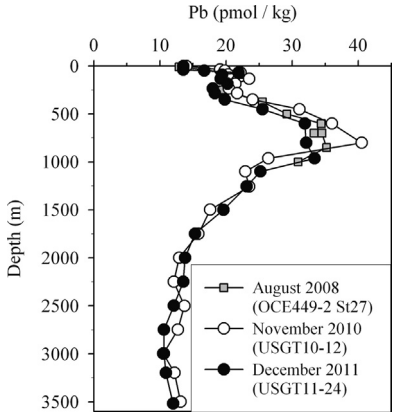

Fig. 12. Profile overlay for USGT10-12 and USGT11-24 that both sampled time series station TENATSO.

dominated by UCDW with some intrusion from ULSW. Although these data are not directly comparable with the Pb data because cast 10 was taken at a different time from the trace metal casts 2 and 7, this sharp change in water mass composition between these depths supports the potential for strong gradients in Pb to exist as well because Pb spatial variability is strongly influenced by ventilation age and water mass. Although these casts clearly sample different water masses, advected Pb from interaction with the sediments along the Eastern Margin could possibly contribute to changes in Pb concentration from one sampling to the next as USGT10-09 is the station closest to the African Margin. Similar (though less dramatic) intermediate depth variability could also be responsible for differences observed among the reoccupations of station TENATSO.

3.9. Remobilization of anthropogenic Pb in bottom waters?

At several stations from the USGT10 expedition (USGT10-05, USGT10-07, USGT10-09, USGT10-11), the deepest samples were characterized by elevated Pb concentrations (Fig. 2W, Y, Z, AA) and the most pronounced of these concentration maxima were characterized by the lowest $^{206}Pb/^{207}Pb$ isotope ratios observed among all samples from both expeditions (USGT10-05, 07, 09, Fig. 4J, I, H). All of these stations were sampled to within ~25 m of the seafloor and some (USGT10-05, USGT10-07, USGT10-09, USGT10-10, and USGT10-11) were characterized by a thin nepheloid layer, as indicated by suppressed transmittance. We suggest that this feature may be caused by release of Pb from fine, recently deposited particles containing anthropogenic Pb from bottom surface sediments. The low $^{206}Pb/^{207}Pb$ anomaly is likely a result of this scavenged Pb having a European/North African source. Deep water masses passing over these sites were generally characterized by low concentrations (10–20 pmol/kg) and relatively high $^{206}Pb/^{207}Pb$ ratios (1.180–1.185), but resuspended particulate Pb in the $<0.2\,\mu m$ size fraction could carry a low $^{206}Pb/^{207}Pb$ ratio given the proximity of these stations to Europe and North Africa and the timescale of Pb scavenging. If Pb had been scavenged by adsorption onto iron and manganese phases, and if these carrier particles are reductively dissolved in the sediments, this released Pb could diffuse into bottom waters.

In contrast to the features observed along the eastern margin, the western margin was characterized by clearly defined, intense and

thick benthic nepheloid layers at USGT11-06 and USGT11-08. The isotopic signature of these waters was also influenced by anthropogenic inputs; however, the concentrations were exceptionally low. A thick nepheloid layer may serve as a more efficient sink for Pb than the thinner, compressed nepheloid layer in the eastern margin. Waters pass through the deep western boundary more quickly than along the eastern margin, and may have less time to accumulate Pb released from the sediments if these waters are replaced quickly by the fast moving boundary current. Analysis of the composition of these particles suggests that samples along the eastern margin are notably different from those along the western boundary, with the eastern margin sediments being composed primarily of calcium carbonates, whereas the western boundary suspended particles were more lithogenic in nature (Lam et al., 2015). Given the redox environment and respective sensitivities of these particles to dissolution, there should be differences in fluxes along the two margins. Pb is chalcophilic, but it is unclear whether the adsorptive processes associated with oxic Pb scavenging may be affected by the composition of the particulate carrier phase.

4. Conclusions

The phaseout of alkyl leaded gasoline in the US and Europe has led to a consistent and dramatic decrease in Pb concentrations in the upper Atlantic Ocean on a decadal timescale. Evidence from this study shows that concentrations are still decreasing, and will likely continue to do so. Because the U.S. was the dominant source of Pb into the North Atlantic for many years, the deeper waters are dominated by a high $^{206}Pb/^{207}Pb$ U.S. signature. Comparison to SF_6 ages shows that the evolution of Pb in subducted waters is consistent with peak Pb in the late 1970s and early 1980s. This study also records the first observation of a shallow Pb and Pb isotope feature within Subtropical Underwater (STUW), and we observe Pb with a low $^{206}Pb/^{207}Pb$ isotope ratio at the STUW source region near the center of the North Atlantic Subtropical Gyre. The feature appears sporadically in our profiles, and highlights the importance of short temporal and spatial scale variability on scales that previously had not been considered for such narrow features. This observation may have implications for other metal micronutrients that could be similarly transported within this thin filamental water mass. Short-term variability on this scale was also observed in intermediate water within the Mauritanian Upwelling, evidenced by a clear offset in both isotopes and concentration between two casts that overlapped the same depth range at USGT10-09. Lastly deep water features revealed a relatively confined source of anthropogenic Pb from bottom sediments along the eastern margin, a scavenging sink within the TAG Hydrothermal plume, and evidence that dissolved Pb does not reach isotopic equilibrium with suspended particles along the western boundary. Ultimately, this study highlights the dynamic variability of Pb and Pb isotopes in this highly affected basin, and demonstrates the utility of Pb in constraining water masses and ocean biogeochemical cycling.

Acknowledgements

This work would not have been possible without the efforts of the GEOTRACES sampling team: Geo Smith, Peter Morton, Jessica Fitzsimmons, Rachel Shelley, Randelle Bundy, Ana Aguilar-Islas, Mariko Hatta, and Chris Measures. We would like to thank the captain and crew of the R/V KNORR for their tireless work and support. We also thank the MIT trace metal team – Jong-Mi Lee, Jessica Fitzsimmons, and Gonzalo Carrasco – for bottle leaching and other cruise preparations. We would also like to thank Simone Moos for helpful discussions on Mediterranean Outflow. We acknowledge the contribution of our co-PIs Bill Jenkins and Greg Cutter in the cruise management. This research was supported by National Science Foundation grants OCE-0926204, OCE-0926197, OCE-0928612 and OCE-1132545.

References

Alleman, L.Y., Véron, A.J., Church, T.M., Flegal, A.R., Hamelin, B., 1999. Invasion of the abyssal North Atlantic by modern anthropogenic lead. Geophys. Res. Lett. 26 (10), 1477–1480.
Alleman, L.Y., Church, T.M., Véron, A.J., Kim, Hamelin, G.B., Flegal, A.R., 2001a. Isotopic evidence of contaminant lead in the South Atlantic troposphere and surface waters. Deep Sea Res. Part II 48, 2811–2827.
Alleman, L.Y., Church, T.M., Ganguli, P., Véron, A.J., Hamelin, B., Flegal, A.R., 2001b. Role of oceanic circulation on contaminant lead distribution in the South Atlantic. Deep Sea Res. Part II 48, 2855–2876.
Bacon, M.P., Spencer, D.W., Brewer, P.G., 1976. 210Pb/226Ra and 210Po/210Pb disequilibria in seawater and suspended particulate matter. Earth Planet. Sci. Lett. 32, 277–296.
Bacon, M.P., Anderson, R.F., 1982. Distribution of thorium isotopes between dissolved and particulate forms in the deep sea. J. Geophys. Res. Oceans 87 (C3), 2045–2056.
Baker, J., Peate, D., Waight, T., Meyzena, C., 1987. Pb isotopic analysis of standards and samples using a 207Pb–204Pb double spike and thallium to correct for mass bias with a double-focusing MC–ICP–MS. Chem. Geol. 211, 275–303.
Bergquist, B.A., Blum, J.D., 2007. Mass-dependent and independent fractionation of Hg isotopes by photoreduction in aquatic systems. Science 318, 417–420.
Boyle, E.A., Chapnick, S.D., Shen, G.T., Bacon, M.P., 1986. Temporal variability of lead in the western North Atlantic. J. Geophys. Res. Oceans 91 (C7), 8573–8593.
Boyle, E.A., Sherrell, R.M., Bacon, M.P., 1994. Lead variability in the western North Atlantic Ocean and central Greenland ice: implications for the search for decadal trends in anthropogenic emissions. Geochim. Cosmochim. Acta 58 (15), 3227–3238.
Boyle, E.A., Lee, J.-M., Echegoyen, Y., Noble, A., Moos, S., Carrasco, G., Zhao, N., Kayser, R., Zhang, J., Gamo, T., Obata, H., Norisuye, K., 2014. Anthropogenic lead emissions in the ocean—the evolving global experiment. Oceanography (March 2014).
Callender, E., Van Metre, P.C., 1997. Reservoir sediment cores show U.S. Lead Declines. Environ. Sci. Tech. 31 (9), 424A–428A.
Copin-Montegut, G., Courau, P., Nicolas, E., 1986. Distribution and transfer of trace elements in the Western Mediterranean. Mar. Chem. 18 (2), 189–195.
Cutter, G.A., Bruland, K.W., 2012. Rapid and noncontaminating sampling system for trace elements in global ocean surveys. Limnol. Oceanogr. Methods 10, 425–436.
Chow, T.J., Patterson, C.C., 1962. The occurrence and significance of lead isotopes in pelagic sediments. Geochim. Cosmochim. Acta 26 (2), 263–308.
Church, T.M., Véron, A., Patterson, C.C., Settle, D., Erel, Y., Maring, H.R., Flegal, A.R., 1990. Trace elements in the North Atlantic troposphere, Shipboard results of precipitation and aerosols. Global Biogeochem. Cycles 4 (4), 431–443.
Desenfant, F., Véron, A.J., Camoin, G.F., Nyberg, J., 2006. Reconstruction of pollutant lead invasion into the tropical North Atlantic during the twentieth century. Coral Reefs 25 (3), 473–484.
Doe, R.B., 1970. Lead Isotopes. Springer, Berlin.
Erel, Y., Dayan, U., Rabi, R., Rudich, Y., Stein, M., 2006. Trans boundary transport of pollutants by atmospheric mineral dust. Environ. Sci. Technol 40, 2996–3005.
Erel, Y., Kalderon-Asael, B., Dayan, U., Sandler, A., 2007. European Atmospheric Pollution Imported by Cooler Air Masses to the Eastern Mediterranean during the summer. Environ. Sci. Technol. 41, 5198–5203.
Fine, R.A., Rhein, M., Andrié, C., 2002. Using a CFC effective age to estimate propagation and storage of climate anomalies in the deep western North Atlantic Ocean. Geophys. Res. Lett 29 (24), 2227.
Fine, R.A., 2011. Observations of CFCs and SF6 as ocean tracers. Annu. Rev. Mar. Sci. 3, 173–195.
Godfrey, L.V., Mills, R., Elderfield, H., Gurvich, E., 1994. Lead behaviour at the TAG hydrothermal vent field, 26¬∞N, Mid-Atlantic Ridge. Mar. Chem. 46 (3), 237–254.
Hopper, J.F., Ross, H.B., Sturges, W.T., Barrie, L.A., 1991. Regional source discrimination of atmospheric aerosols in Europe using the isotopic composition of lead. Tellus Ser. B 43 (1), 45–60.
Hamelin, B., Grousset, F., Sholkovitz, E.R., 1990. Pb isotopes in surficial pelagic sediments from the North Atlantic. Geochim. Cosmochim. Acta 54 (1), 37–47.
Hamelin, B., Ferrand, J.L., Alleman, L., Nicolas, E., Véron, A., 1997. Isotopic evidence of pollutant lead transport from North America to the subtropical North Atlantic gyre. Geochim. Cosmochim. Acta 61 (20), 4423–4428.
Helmers, E., Mart, L., Schulz-Baldes, M., Ernst, W., 1990. Temporal and spatial variations of lead concentrations in Atlantic surface waters. Mar. Pollut. Bull. 21, 515–518.
Helmers, E., Mart, L., Schrems, O., 1991. Lead in Atlantic surface waters as a tracer for atmospheric input. Fresenius J. Anal. Chem. 340, 580–584.
Helmers, E., van. der. Loeff, M.M.R., 1993. Lead and aluminum in Atlantic surface waters (50°N to 50°S) reflecting anthropogenic and natural sources in the eolian transport. J. Geophys. Res. 98, 20261–20273.

Hurst, R.W., 2002. Lead isotopes as age-sensitive genetic markers in hydrocarbons. 3. Leaded Gasoline, 1923-1990 (ALAS model). Environ. Geosci. 9, 43–50.
Jenkins, W.J., Smethie Jr., W.M., Boyle, E.A., Cutter, G.A., 2015. Water mass analysis for the U.S. GEOTRACES North Atlantic Sections. Deep Sea Res. II 116, 6–20. http://dx.doi.org/10.1016/j.dsr2.2014.11.018.
Kelly, A.E., Reuer, M.K., Goodkin, N.F., Boyle, E.A., 2009. Lead concentrations and isotopes in corals and water near Bermuda, 1780–2000. Earth Planet. Sci. Lett. 283 (1,Äì4), 93–100.
Krogh, T.E., 1973. A low-contamination method for hydrothermal decomposition of zircons and extraction of U and Pb for isotopic age determinations. Geochim. Cosmochim. Acta 37, 485–494.
Kuhlbrodt, T., Griesel, A., Montoya, M., Levermann, A., Hofmann, M., Rahmstorf, S., 2007. On the driving processes of the Atlantic meridional overturning circulation. Rev. Geophys. 45 (2), RG2001.
Kumar, A., Abouchami, W., Galer, S.J.G., Garrison, V.H., Williams, E., Andreae, M.O., 2014. A radiogenic isotope tracer study of transatlantic dust transport from Africa to the Caribbean. Atmos. Environ 82, 130–143.
Lacombe, H., Gascard, J., Gonella, J., Bethoux, J., 1981. Response of the Mediterranean to the water and energy fluxes across its surface, on seasonal and interannual scales. Oceanolog. Acta 4 (2), 247–255.
Lam, P.J., Ohnemus, D.C., Auro, M.E., 2015. Size fractionated major particle composition and mass from the US GEOTRACES North Atlantic Zonal Transect. Deep Sea Res. II 116, 303–320. http://dx.doi.org/10.1016/j.dsr2.2014.11.020.
Lambert, C.E., Nicolas, E., Véron, A., Buatmenard, P., Klinkhammer, G., Lecorre, P., Morin, P., 1991. Anthropogenic lead cycle in the northeastern Atlantic. Oceanolog. Acta 14 (1), 59–66.
Laumond, F., Copinmontegut, G., Courau, P., Nicolas, E., 1984. Cadmium, copper, and lead in the western Mediterranean Sea. Mar. Chem. 15 (3), 251–261.
Lee, J.-M., Boyle, E.A., Echegoyen-Sanz, Y., Fitzsimmons, J.N., Zhang, R., Kayser, R.A., 2011. Analysis of trace metals (Cu, Cd, Pb, and Fe) in seawater using single batch nitrilotriacetate resin extraction and isotope dilution inductively coupled plasma mass spectrometry. Anal. Chim. Acta 686, 93–101.
Manhes, G., Minster, J.F., Allegre, C.J., 1978. Comparative uranium–thorium–lead and rubidium–strontium study of the Saint Severin amphoterite, consequences for early solar system chronology. Earth Planet. Sci. Lett. 39 (1), 14–24.
Mantyla, A.W., Reid, J.L., 1983. Abyssal characteristics of the world ocean waters. Deep Sea Res. Part A 30 (8), 805–833.
Moos, S.B., Boyle, E.A., 2014. Trace metal concentrations (Ba, Cd, Cu, Ni, Pb, Zn) and Pb isotopic signatures throughout the 1980s surface Mediterranean Sea and the deep Alboran Sea. Marine Chem., (in preparation).
Nozaki, Y., Thomson, J., Turekian, K.K., 1976. The distribution of Pb-210 and Po-210 in the surface waters of the Pacific Ocean. Earth Planet. Sci. Lett. 32, 304–312.
Nriagu, J.O., 1979. Global inventory of natural and anthropogenic emissions of trace metals to the atmosphere. Nature 279 (5712), 409–411.
O'Connor, B.M., Fine, R.A., Olson, D.B., 2005. A global comparison of subtropical underwater formation rates. Deep Sea Res. Part I 52 (9), 1569–1590.
Ohnemus, D.C., Lam, P.J., 2015. Cycling of lithogenic marine particulates in the US GEOTRACES North Atlantic Zonal Transect. Deep Sea Res. II 116, 283–302. http://dx.doi.org/10.1016/j.dsr2.2014.11.019.
Pickart, R.S., 1992. Water mass components of the North Atlantic deep western boundary current. Deep Sea Res. 39 (9), 1553–1572.
Rehkamper, M., Frank, M., Hein, J.R., Porcelli, D., Halliday, A., Ingric, J., Liebetrau, 2002. Thallium isotope variations in seawater and hydrogenetic, diagenetic, and hydrothermal ferromanganese deposits. Earth Planet. Sci. Lett. 197, 65–81.
Reuer, M.K., Boyle, E.A., Grant, B.C., 2003. Lead isotope analysis of marine carbonates and seawater by multiple collector ICP–MS. Chem. Geol. 2003 (1), 137–153.
Rutgers van der Loeff, M.M., van Bennekom, A.J., 1989. Weddell sea contributes little to silicate enrichment in Antarctic Bottom Water. Deep Sea Res. Part A 36 (9), 1341–1357.
Schaule, B.K., Patterson, C.C., 1981. Lead concentrations in the northeast Pacific, evidence for global anthropogenic perturbations. Earth Planet. Sci. Lett. 54 (1), 97–116.
Schaule, B.K., Patterson, C.C., 1983. Perturbations of the natural lead depth profile in the Sargasso Sea by Industrial Lead. In: Wong, C.S., et al. (Eds.), Trace Metals in Seawater. Plenum, pp. 487–504.
Schlitzer, R., 2007. Assimilation of radiocarbon and chlorofluorocarbon data to constrain deep and bottom water transports in the world ocean. J. Phys. Oceanogr 37 (2), 259–276.
Shen, G.T., Boyle, E.A., 1988. Thermocline ventilation of anthropogenic lead in the western North Atlantic. J. Geophys. Res. 93 (C12), 15715–15732.
Sherrell, R.M., Boyle, E.A., Hamelin, B., 1992. Isotopic equilibration between dissolved and suspended particulate lead in the Atlantic Ocean, Evidence from 210Pb and stable Pb isotopes. J. Geophys. Res. 97 (C7), 11257–11268.
Shotyk, W., et al., 2005. Predominance of industrial Pb in recent snow (1994–2004) and ice (1842–1996) from Devon Island, Arctic Canada. Geophys. Res. Lett 32 (21), L21814.
Simonetti, A., Gariépy, C., Carignan, J., 2000a. Pb and Sr isotopic evidence for sources of atmospheric heavy metals and their deposition budgets in northeastern North America. Geochim. Cosmochim. Acta 64 (20), 3439–3452.
Simonetti, A., Gariépy, C., Carignan, J., 2000b. Pb and Sr isotopic compositions of snowpack from Québec, Canada, inferences on the sources and deposition budgets of atmospheric heavy metals. Geochim. Cosmochim. Acta 64 (1), 5–20.
Simonetti, A., Gariépy, C., Carignan, J., 2003. Tracing sources of atmospheric pollution in Western Canada using the Pb isotopic composition and heavy metal abundances of epiphytic lichens. Atmos. Environ 37 (20), 2853–2865.
Stramma, L., Hüttl, S., Schafstall, J., 2005. Water masses and currents in the upper tropical northeast Atlantic off northwest Africa. J. Geophys. Res. Oceans 110 (C12), C12006.
Stramma, L., Schott, F., 1999. The mean flow field of the tropical Atlantic Ocean. Deep Sea Res. Part II 46 (1), 279–303.
Tomczak, M., 1981. A multi-parameter extension of temperature/salinity diagram techniques for the analysis of non-isopycnal mixing. Prog. Oceanogr 10, 147–171.
Thirwall, M.F., 2000. Inter-laboratory and other errors in Pb isotope analysis investigated using a 207Pb/204Pb double spike. Chem. Geol. 163, 299–322.
Trefry, J.H., Metz, S., Trocine, R.P., 1985. A decline in lead transport by the Mississippi River. Science 230, 439–441.
Turekian, K.K., 1977. The fate of metals in the oceans. Geochim. Cosmochim. Acta 41 (8), 1139–1144.
van Geen, A., Rosener, P., Boyle, E., 1988. Entrainment of trace-metal-enriched Atlantic-shelf water in the inflow to the Mediterranean Sea. Nature 331, 4.
Véron, A., Lambert, C.E., Isley, A., Linet, P., Grousset, F., 1987. Evidence of recent lead pollution in deep Northeast Atlantic sediments. Nature 326 (6110), 278–281.
Véron, A., Church, T.M., Patterson, C.C., Erel, Y., Merrill, J.T., 1992. Continental origin and industrial sources of trace metals in the Northwest Atlantic troposphere. J. Atmos. Chem. 14 (1-4), 339–351.
Véron, A.J., Church, T.M., Flegal, A.R., Patterson, C.C., Erel, Y., 1993. Response of lead cycling in the surface Sargasso Sea to changes in tropospheric input. J. Geophys. Res. 98, 18269–18276.
Véron, A.J., Church, T.M., Patterson, C.C., Flegal, A.R., 1994. Use of stable lead isotopes to characterize the sources of anthropogenic lead in North Atlantic surface waters. Geochim. Cosmochim. Acta 58 (15), 3199–3206.
Véron, A.J., Church, T.M., 1997. Use of stable lead isotopes and trace metals to characterize air mass sources into the eastern North Atlantic. J. Geophys. Res. 102 (D23), 28049–28058.
Véron, A.J., Church, T.M., Flegal, A.R., 1998. Lead isotopes in the Western North Atlantic, transient tracers of pollutant lead inputs. Environ. Res. 78 (2), 104–111.
Véron, A.J., Church, T.M., Rivera-Duarte, I., Flegal, A.R., 1999. Stable lead isotopic ratios trace thermohaline circulation in the subarctic North Atlantic. Deep Sea Res. Part II 46 (5), 919–935.
Weiss, D., et al., 2003. Spatial and temporal evolution of lead isotope ratios in the North Atlantic Ocean between 1981 and 1989. J. Geophys. Res. Oceans 108 (C10), 3306.
Wu, J.F., Boyle, E.A., 1997. Lead in the western North Atlantic Ocean, completed response to leaded gasoline phaseout. Geochim. Cosmochim. Acta 61, 3279–3283.
Wu, J., Rember, R., Jin, M., Boyle, E.A., Flegal, A.R., 2009. Isotopic evidence for the source of lead in the North Pacific abyssal water. Geochim. Cosmochim. Acta 74 (16), 4629–4638.